## Shifting Consensus in a Biased Compromise Model\*

Olivia Cannon<sup>†</sup>, Ty Bondurant<sup>‡</sup>, Malindi Whyte<sup>§</sup>, and Arnd Scheel<sup>†</sup>

Abstract. We investigate the effect of bias on the formation and dynamics of opinion clusters in the bounded confidence model. For weak bias, we quantify the change in average opinion and potential dispersion and decrease in cluster size. For nonlinear bias modeling self-incitement, we establish coherent drifting motion of clusters on a background of uniform opinion distribution for biases below a critical threshold where clusters dissolve. Technically, we use geometric singular perturbation theory to derive drift speeds, we rely on a nonlocal center manifold analysis to construct drifting clusters near threshold, and we implement numerical continuation in a forward-backward delay equation to connect asymptotic regimes.

**Key words.** social dynamics, coherent structures, bounded confidence, traveling waves, lattice dynamical systems, nonlocal expansion

MSC codes. 37N99, 34A33, 37G99

**DOI.** 10.1137/23M1552346

1. Introduction. Bounded confidence models [20] have been pivotal in the study of social dynamics, providing a mechanism for the formation of opinion clusters, in some contexts referred to as parties. Agents are attributed numerical values of opinions. They interact and change their opinions through compromise, but only with other agents whose opinions are sufficiently close, i.e., within a bounded confidence interval. These models can be framed in many different formulations—stochastic Markov processes, deterministic mean-field equations, discrete or continuous opinion values—but the qualitative phenomena are similar: a uniform distribution of opinions is an unstable steady state, and small fluctuations from the uniform state lead to the formation of clusters, often regularly spaced [4, 5, 6, 18, 20, 23, 29, 30].

Bounded confidence models have been used in large part to study mechanisms of polarization, and to that end, many modifications have been made, including, for instance, variations of the confidence interval between agents, introduction of a small number of agents who do not compromise ("stubborn" agents), and variations in the probability of interaction [9, 11, 12, 14, 19, 27, 33, 36, 38]. The present work is concerned with *drift* of opinion clusters, that is, with the continuous movement of clusters toward one extreme of the opinion spectrum. While drift caused by asymmetric confidence has been reported in [20, section 4.2], there appear to be few systematic computational or analytical studies of this phenomenon.

<sup>\*</sup>Received by the editors February 9, 2023; accepted for publication (in revised form) August 4, 2023; published electronically January 22, 2024.

https://doi.org/10.1137/23M1552346

Funding: This work was partially supported through grants NSF DMS-1907391 and NSF DMS-2205663.

<sup>&</sup>lt;sup>†</sup>School of Mathematics, University of Minnesota, Minneapolis, MN 55455 USA (canno238@umn.edu, scheel@umn.edu).

<sup>&</sup>lt;sup>‡</sup>School of Mathematics, Georgia Institute of Technology, Atlanta, GA 30332 USA (tbondurant3@gatech.edu).

<sup>&</sup>lt;sup>§</sup>Department of Mathematics, Wake Forest University, Winston-Salem, NC 27109 USA (whytmg19@wfu.edu).

We are interested in this effect as a self-organized phenomenon, caused by behavioral bias in individual agents. We model this through the addition of bias terms to the bounded confidence model. We will demonstrate how bias terms typically lead to drift of average opinions in a cluster but may also lead to disintegration of individual clusters. Our focus therefore will be on a nonlinear quadratic bias term that corresponds to self-incitement and which leads to both persistent and coherent drift, avoiding in particular dispersal and disintegration.

The focus on this particular form of bias is also rooted in its relevance as a model for the common sociological phenomenon of group polarization [25]. Starting with the observation of James Stoner in 1961, it was noted that groups often collectively form an opinion more extreme than the average of the individual opinions. This phenomenon is now broadly supported and has been found to be present in a large variety of contexts, including group decisions, social networks, games, juries, corporate boards, and in studies in numerous countries and cultural contexts [25, 26, 31, 34, 35, 39, 43]. Various mechanisms for group polarization have been proposed and have remained in question, including interpersonal comparison and social motivation, informational influence, and group decision rules. Notably, a study by Van Swol found that the shift in group opinion was independent of the presence of extremist group members [41], and, furthering this point, earlier studies had already established independence from the skew of the group opinions [35]. This suggests that the mechanism of self-incitement, or the interaction between agents at the same opinion site, may quite accurately reflect mechanisms underlying opinion shift.

In particular, we study the following deterministic mean-field model for the evolution of populations of agents  $P_n$  with opinion  $n \in \mathbb{Z}$ :

(1.1) 
$$\frac{dP_n}{dt} = 2P_{n+1}P_{n-1} - P_n(P_{n+2} + P_{n-2}) + \beta(P_{n+1}^2 - P_n^2), \qquad n \in \mathbb{Z}.$$

Here,  $\beta = 0$  corresponds to a deterministic Hegselmann–Krause-style bounded-confidence model in continuous time on a lattice, where populations  $P_{n-1}$  and  $P_{n+1}$  interact with mass-action rates to form opinions  $P_n$ . We added the self-incitement bias term  $\beta(P_{n+1}^2 - P_n^2)$ , which can be interpreted as that an individual agent decreases their opinion value by one with probability proportional to the population size with the same opinion: interactions between "same-opinion agents" lead to opinion drift toward the extreme. The strength of the bias term is encoded in the parameter  $\beta > 0$ .

Our results for this model can roughly be summarized as follows:

- (i) There exists a critical bias level  $\beta_{\text{crit}} = 2$ , such that for  $\beta > \beta_{\text{crit}}$ , formation of opinion clusters is suppressed and uniform distribution of opinions is stable.
- (ii) For weak bias  $\beta \gtrsim 0$ , drift speeds c are at leading order proportional to bias and cluster mass,  $c \sim \frac{2\beta m}{\pi}$ .
- (iii) For subcritical, strong bias close to criticality,  $\beta \lesssim \beta_{\rm crit} = 2$ , we establish rigorously coherent cluster drift on a constant background of size m with speed  $c \sim 4m$ .
- (iv) For bias  $0 < \beta < 2$ , we find drifting clusters by numerical continuation and find that the background population that supports coherent cluster drift is exponentially small,  $\exp(-\cosh/\beta)$ .

The results in (i)–(iii) are analytical. Only in the regime (iii) are we able to establish existence of coherent cluster drift, while (ii) leaves open the possibility of eventual dispersal of a

cluster. We also briefly discuss some intriguing phenomena related to stability and instability of drifting clusters.

Technically, the results in (ii) rely on a leading order computation of a flow on a slow manifold using geometric singular perturbation theory, while (iii) uses a recently introduced novel method for analyzing coherent structures in nonlocally coupled equations.

Outline. In section 2, we collect information about the bounded confidence model and the model with bias terms added, as well as the linearization at single-cluster and uniform states. We establish in section 3 the speed of drift for  $\beta \ll 1$ , case (ii), using methods from geometric singular perturbation theory. The  $\beta \nearrow 2$  regime, case (iii), is treated in section 4, where drifting solutions are established using nonlocal methods. In section 5, we describe numerical approaches and results, in particular concerning case (iv) above. Section 6 describes numerical evidence for lack of coherence when the equation is posed with other bias terms. We conclude with a brief discussion.

2. The bounded confidence model: Equilibria, stability, and bias. The bounded confidence model

(2.1) 
$$\frac{dP_n}{dt} = 2P_{n+1}P_{n-1} - P_n(P_{n+2} + P_{n-2}), \qquad P_n \geqslant 0, \ n \in \mathbb{Z},$$

describes the dynamics of an opinion distribution  $P_n(t)$ ,  $n \in \mathbb{Z}$ , where  $P_n(t)$  represents the local population size with opinion n at time t. Agents at sites n-1 and n+1 compromise through interaction, moving to opinion n, while agents at site n compromise with those at n+2 and n-2, leaving site n. There is no interaction between agents at a distance greater than 2. The equation clearly preserves mass and average opinion (or first moment),

$$\frac{d}{dt}\sum_{n}P_{n}=0,$$
  $\frac{d}{dt}\sum_{n}nP_{n}=0,$ 

provided reasonable conditions such as sufficient localization at  $|n| \to \infty$ . The dynamics of (2.1) are to some extent understood. The consensus process leads to the formation of opinion clusters, which one refers to as clusters. For (2.1), these clusters can be supported on one or two opinions sites, that is, for instance,  $P_0 = 1$ ,  $P_j = 0$  for  $j \neq 0$ , or  $P_0 = \alpha$ ,  $P_1 = 1 - \alpha$ ,  $P_j = 0$  for  $j \notin \{0,1\}$ . Clusters separated by at least two empty sites between them will not interact, and one can in this fashion generate equilibrium states with multiple clusters. Opinion clusters, once well established after initial transients, appear to be very robust, although introduction of agents away from existing clusters may lead to the formation of new clusters. In addition to these single-cluster states, supported on one or two opinion sites, and the associated well separated multi-cluster states, the equation also supports equilibria of uniform opinion distribution,  $P_n \equiv m$  for all m. We refer the reader to [4] for background on the model and its dynamics. We note, however, that many questions of stability have not been answered in a precise mathematical fashion, possibly due to the abundance and complexity of possible equilibrium configurations.

**2.1. Single-cluster states.** A single two-site cluster of mass m takes the form  $P_{\alpha,n}^* = (0,\ldots,\overset{\downarrow n}{m}\alpha,m(1-\alpha),\ldots,0)^{\perp}$  for  $\alpha\in(0,1)$ . In the limiting case  $\alpha=0$  or  $\alpha=1$ , the cluster

only occupies one site. It represents (total) consensus of opinion at two adjacent opinion sites n and n+1. The linearized vector field at a two-site and at a one-site equilibrium ( $\alpha = 0$ ) of (2.1) with mass m=1 are, respectively, given by the matrices

By scaling invariance, linearization at clusters with mass m gives the same matrices multiplied by a factor m.

Both matrices clearly have infinite-dimensional kernels, with bases spanned by

$$\{e_j \mid j \neq n-2, n-1, n+2, n+3\}$$
 and  $\{e_j \mid j \neq n-2, n+2\}$ ,

respectively. Here,  $e_n$  is the canonical basis vector such that  $(e_n)_k = \delta_{nk}$  with Kronecker- $\delta$  notation.

For the two-site cluster, the kernel has codimension 4 and corresponds to the two sites of the cluster and the sites at a distance 3 or more away. The spectrum of the linearization is  $\{0, -m\alpha, m(1-\alpha)\}$ . For the one-site cluster, the kernel has codimension 2 and the spectrum of the linearization is  $\{0, -m\}$ . The complement of the kernel can be associated with opinion sites n that interact with the support of the cluster, while kernel elements correspond to lattice sites that do not interact with the cluster, either because they are too far away or because they simply change the shape of the cluster.

Associated with the kernel elements  $e_n$  and  $e_{n+1}$  for the two-site cluster, there is a two-dimensional family of single cluster equilibria parameterized by the mass m and the parameter  $\alpha$ , which can be thought of as parameterizing the average opinion in the cluster. At the two-site

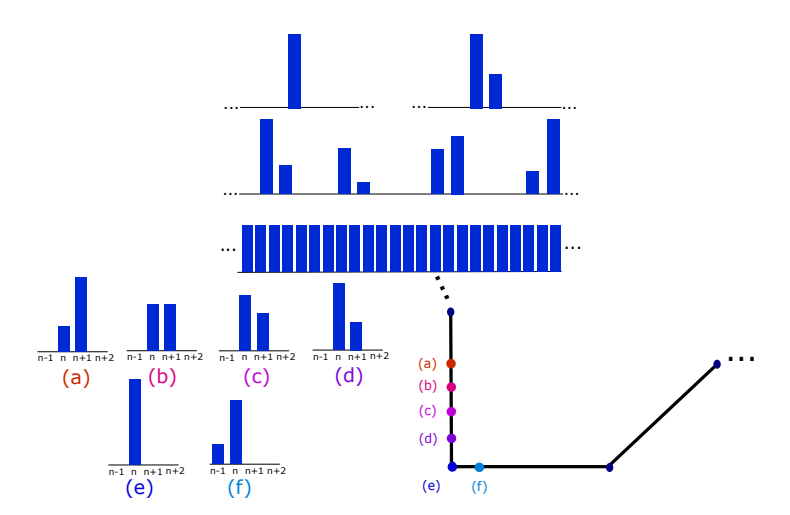


**Figure 2.1.** Single-cluster at one or two sites, multi-cluster, and uniform distribution equilibria (top). Phase-space schematic of a family of single-cluster equilibria with corners at one-site clusters (bottom).

cluster, one can associate the kernel vector  $e_n$  with mass change and the kernel vectors  $e_{n+1}$  and  $e_{n-1}$  with increases or decrease in the average opinion in the cluster. Note, however, that the direction  $e_{n+1} + e_{n-1}$  associated with states  $(\dots, 0, 0, \alpha, 1, \alpha, 0, 0, \dots)^{\perp}$  does not correspond to the tangent space of a family of equilibria. Similarly, directions in the kernel with support on more than two sites do not correspond to families of equilibria. In particular, the infinite-dimensional kernel is *not* simply the tangent space to a high-dimensional family of equilibria, a fact that will slightly complicate the application of singular perturbation theory later. We remark that the stability of single-cluster states is analytically rather subtle due to this high-dimensional kernel and the possible associated dynamics of clustering of small mass nearby in phase space but far away in the opinion spectrum.

Fixing total mass, single-cluster states naturally come in a one-parameter family  $\mathcal{F}$  that can be parameterized by their average opinion: A cluster with mass  $1-\alpha$  at site n and mass  $\alpha$  at site n+1 has average opinion  $n+\alpha$ .

Drifting opinion in a biased model is to leading order described by drift along this continuous family of single-cluster states. A subtlety arises when viewing this family in phase space. The tangent vector to the family of two-site clusters supported on sites n and n+1 is  $e_n - e_{n+1}$ . This tangent vector is discontinuous at the one-site cluster, where the continuous curve of single-cluster equilibria possesses a corner; see Figure 2.1 for an illustration. Drift along this corner, as we shall see below, introduces dynamics and error terms known from the analysis of a passage through a transcritical bifurcation.

**2.2. Uniform distribution of opinions.** The uniform state  $P_n \equiv m$  is also an equilibrium of (2.1). This equilibrium turns out to be unstable, and a typical question of interest is how fluctuations around this equilibrium evolve into multi-cluster states. In order to understand this process, one usually starts by linearizing (2.1) at the uniform state to find

$$\frac{dP_n}{dt} = m(-P_{n-2} + 2P_{n-1} - 2P_n + 2P_{n+1} - P_{n+2}).$$

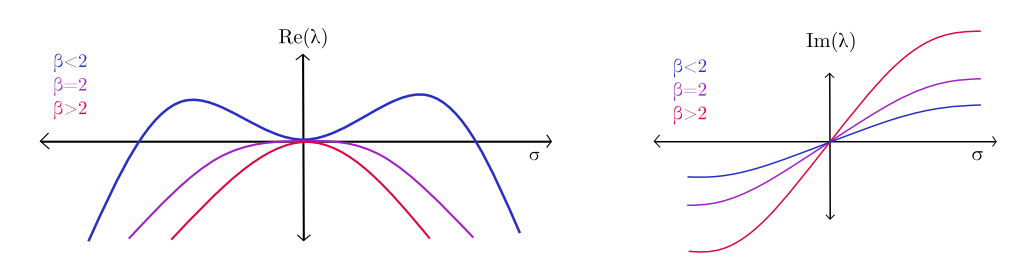


**Figure 2.2.** Linear dispersion relation (2.3) for  $\beta < 2$ ,  $\beta = 2$ , and  $\beta > 2$ .

Solutions to this constant-coefficient lattice-differential equation can readily be found after Fourier transform. Therefore, inserting an ansatz  $P_n = e^{i\sigma n + \lambda t}$ , one finds the dispersion relation

$$\lambda = 2m(2\cos(\sigma) - \cos(2\sigma) - 1), \quad -\pi \leqslant \sigma < \pi;$$

see also Figure 2.2. The temporal eigenvalue  $\lambda$  is real and obtains a maximum of 1 at  $\sigma = \pm \frac{\pi}{3}$ . The linearization therefore predicts fastest growth of perturbations with period n=6, predicting that white-noise fluctuations around a constant state would evolve towards a multicluster state with peaks at sites with distance  $\delta n = 6$ . A more refined branch point analysis of this dispersion relation reveals that localized perturbations of the unstable state evolve into clusters with different spacing,  $\delta n = 5.311086...$ ; see [5]. We will return to this analysis when considering stability of uniform states with (strong) bias.

**2.3.** The effect of bias on equilibria. Returning to the model equation with self-incitement bias,

(2.2) 
$$\frac{dP_n}{dt} = 2P_{n+1}P_{n-1} - P_n(P_{n+2} + P_{n-2}) + \beta(P_{n+1}^2 - P_n^2),$$

we note that, for  $\beta > 0$ , single-cluster states do not form equilibria. The resulting drift of single clusters along the family of equilibria  $\mathcal{F}$  with a resulting change in average opinion is the object of much of the remainder of this paper.

On the other hand, the uniform state does persist as an equilibrium, but the linearization picks up new terms. When  $\beta > 0$ , the linearized equation

$$\frac{dP_n}{dt} = m(-P_{n-2} + 2P_{n-1} - (2+2\beta)P_n + (2+2\beta)P_{n+1} - P_{n+2})$$

has dispersion relation

(2.3) 
$$\lambda = m(-2\cos(2\sigma) + (4+2\beta)\cos(\sigma) - (2+2\beta) + 2i\beta\sin(\sigma)).$$

For  $\beta < 2$ , the maximum of  $\operatorname{Re}\lambda(\sigma)$  is positive and the uniform state is unstable. However, for  $\beta \geq 2$ ,  $\operatorname{Re}\lambda \leqslant 0$  is nonpositive, with a quadratic tangency of the eigenvalues at the origin for  $\beta > 2$ : strong bias stabilizes uniform distribution of opinion and hence disfavors opinion clusters!

Intuitively, this effect stems from the added advection and diffusion induced by the bias term in the linearization. The negative diffusion in the compromise process competes with positive diffusion from discrete transport, and for high enough bias, the latter dominates and stabilizes the uniform state. Mechanistically, one can intuitivize the high bias as causing movement so fast that agents move outside the compromise region before any cluster can be kept together.

Spectral stability in the dispersion relation translates readily into linear stability in, say,  $\ell^2$ . One would also expect nonlinear stability with approximately diffusive decay of the perturbation for localized initial conditions, measured in  $\ell^{\infty}$ , due to the presence of (discrete) derivatives in the nonlinearity; see Remark 4.1 for more detail.

We shall exploit the change of stability in our bifurcation analysis, showing that the destabilization is accompanied by the creation of localized coherent structures, in section 4.

- 3. Small bias regime. We study here dynamics for  $0 < \beta \ll 1$ . We use methods from geometric singular perturbation theory (GSPT) to investigate the speed of propagation of a single cluster in the biased system. We note that the lack of smoothness of the family of equilibria in the unbiased system prohibits a global slow-fast decomposition using existing theory. Nevertheless, we find locally invariant manifolds and separately analyze the system near the points where the manifold is not smooth, allowing us to compute the local speed of propagation for small bias.
- **3.1. Singular perturbation analysis near single-cluster equilibria.** We begin by establishing the existence of locally invariant manifolds.

Proposition 3.1 (two-site center manifold). Fix  $n \in \mathbb{Z}$ ,  $k \geqslant 1 \in \mathbb{N}$  arbitrary, and  $\delta > 0$  arbitrarily small. Then, for each fixed mass m > 0 of two-site cluster equilibria, there exists a family of locally invariant, infinite-dimensional, codimension-4,  $C^k$ -manifolds  $\mathcal{M}_{\beta} \subset \ell^{\infty}$ , which depend on  $\beta$  in a  $C^k$ -fashion such that  $\mathcal{M}_0 \supset \{P_{\alpha,n}^* \mid \alpha \in (\delta, 1 - \delta)\}$ , the part of the family of two-site single-cluster equilibria supported on sites n and n+1 away from one-site single-cluster equilibria. Its tangent space for  $\beta = 0$  at any of the two-site equilibria coincides with the infinite-dimensional kernel of the linearization at this equilibrium.

*Proof.* The manifold of equilibria  $\mathcal{M}_0$  is (locally) invariant, and its linearization possesses an exponential dichotomy with a four-dimensional stable subspace and an infinite-dimensional center subspace, with uniformly bounded projections  $\mathcal{P}^s$  and  $\mathcal{P}^c$ . Standard theory for invariant manifolds then shows the existence of smooth, locally invariant center manifolds associated with this splitting, using, for instance, graph transforms as in [3, 17, 22].

Proposition 3.2 (one-site center manifold). Fix  $n \in \mathbb{Z}$ ,  $k \geqslant 1 \in \mathbb{N}$  arbitrary, and  $\delta > 0$  sufficiently small. Then, for fixed mass m > 0 of the one-site equilibrium, there exists a family of locally invariant, infinite-dimensional, codimension-2,  $C^k$ -manifolds  $\mathcal{M}'_{\beta} \subset \ell^{\infty}$ , which depend on  $\beta$  in a  $C^k$ -fashion such that  $\mathcal{M}'_0 \supset P_n^* \cup \{P_{\alpha,m}^* \mid m = n, \alpha \in (0, \delta); m = n - 1, \alpha \in (1 - \delta, 1)\}$ , the family of two-site single-cluster equilibria close to the one-site equilibrium  $P_n^*$ . Its tangent space for  $\beta = 0$  at the one-site equilibrium coincides with the infinite-dimensional kernel of the linearization at this equilibrium.

*Proof.* This is a standard local center-manifold result in infinite dimensions; see, for instance, [42, 21]. It contains the family of equilibria since it contains all small solutions bounded for all times.

We emphasize that the two-site center manifold is global in the sense that it contains a compact subset of the line of equilibria between two one-site clusters, while the one-site center manifold is local, defined only in a small neighborhood of the one-site cluster.

**3.2.** Leading-order dynamics away from corners. Using invariance, we can now compute the leading-order dynamics on each manifold and the reduced flow. Away from the corners, we can parameterize the kernel of the linearization at a two-site cluster  $P_{\alpha,n}^*$  through values  $q_n, q_{n+1}$  and  $p \in \ell^{\infty}, p_j = 0$  for  $n-2 \le j \le n+3$  and write the manifold by  $P = h(q_n, q_{n+1}, p, \beta)$ ,

$$h(q_n, q_{n+1}, p, \beta) = (\alpha + q_n)e_n + (1 - \alpha + q_{n+1})e_{n+1} + p + \mathcal{O}(\beta, |q_n|^2 + |q_{n+1}|^2, |p|^2).$$

In this parameterization, we have

$$\dot{q}_n = \beta \mathcal{P}^c(G(h(q_n, q_{n+1}, p, \beta)))_n + \mathcal{O}(\beta^2, |q_n|^2 + |q_{n+1}|^2, |p|^2), 
\dot{q}_{n+1} = \beta \mathcal{P}^c(G(h(q_n, q_{n+1}, p, \beta)))_{n+1} + \mathcal{O}(\beta^2, |q_n|^2 + |q_{n+1}|^2, |p|^2), 
\dot{p} = \mathcal{O}(|p|^2, |\beta p|, \beta^2(|q_n| + |q_{n+1}|)),$$

where  $G(P)_j = P_{j+1}^2 - P_j^2$ , and  $\mathcal{P}^c$  is the spectral projection onto  $\ker Df(P_{\alpha,n}^*)$ , defined as

$$\mathcal{P}^{c}(P)_{j} = \begin{cases} P_{j}, & j < n-2, j > n+3, \\ 0, & j = n+1, n+2, n-1, n-2, \\ 3P_{n-2} + 2P_{n-1} + P_{n} - P_{n+2} - 2P_{n+3}, & j = n, \\ -2P_{n-2} - P_{n-1} + P_{n+1} + 2P_{n+2} + 3P_{n+3}, & j = n+1. \end{cases}$$
w scaling  $p = \beta a$ , we find explicitly at leading order on the center manifold

Now scaling  $p = \beta q$ , we find explicitly at leading order on the center manifold

$$\dot{q}_n = \beta(\alpha^2 + (1 - \alpha)^2) + \mathcal{O}(\beta^2), 
\dot{q}_{n+1} = -\beta((\alpha)^2 + (1 - \alpha)^2) + \mathcal{O}(\beta^2), 
\dot{p} = \mathcal{O}(\beta^2).$$

Clearly, at leading order mass in the cluster is conserved,  $\dot{P}_n + \dot{P}_{n+1} = 0$ . For the family of two-site clusters parameterized by  $P_n = \alpha, P_{n+1} = 1 - \alpha$ , this gives

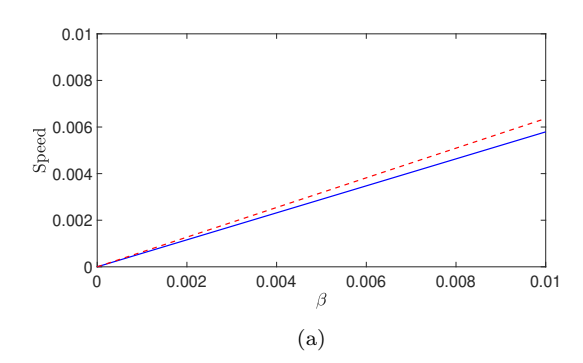
(3.1) 
$$\dot{\alpha} = -\beta \left[\alpha^2 + (1 - \alpha)^2\right] + \mathcal{O}(\beta^2).$$

We compare this first-order approximation (3.1) with numerically computed drift speeds averaged in time, that is, covering the interval  $\alpha \in [0,1]$  rather than the interval  $(\delta, (1-\delta))$ where the above analysis applies in Figure 3.1(a). Details on computational procedures are delineated in section 5. We see that the predicted speeds here give the leading-order term for small  $\beta$ , but the discrepancy for even moderately small values of  $\beta$  is significant. We show how this discrepancy can be attributed to the passage near the one-site clusters, contributing a term  $\beta^{3/2}$ .

3.3. Corner dynamics and slow passage through transcritical bifurcations. We now compute the leading-order dynamics near the one-site cluster. The kernel of the linearization  $Df(P_n^*)$  is now of codimension 2, and we parameterize elements  $P_c$  of the kernel by values  $\alpha_+, \alpha_-, \alpha_m \in \mathbb{R}$  and  $p \in \ell^{\infty}$ , with  $p_j = 0$  for  $n - 2 \le j \le n + 2$ . Let

$$e_{+} = (0, \dots, 1, \stackrel{\downarrow n}{-1}, 0, \dots)^{\perp}, \qquad e_{-} = (0, \dots, 0, \stackrel{\downarrow n}{-1}, 1, \dots)^{\perp}, \qquad e_{m} = (0, \dots, 0, \stackrel{\downarrow n}{1}, 0, \dots)^{\perp},$$

$$e_{+}^{*} = (0, \dots, 0, 0, \stackrel{\downarrow n}{0}, 1, 2 \dots)^{\perp}, \quad e_{-}^{*} = (0, \dots, 2, 1, \stackrel{\downarrow n}{0}, 0, 0, \dots)^{\perp}, \quad e_{m}^{*} = (0, \dots, 1, 1, \stackrel{\downarrow n}{1}, 1, 1, 0 \dots)^{\perp}.$$



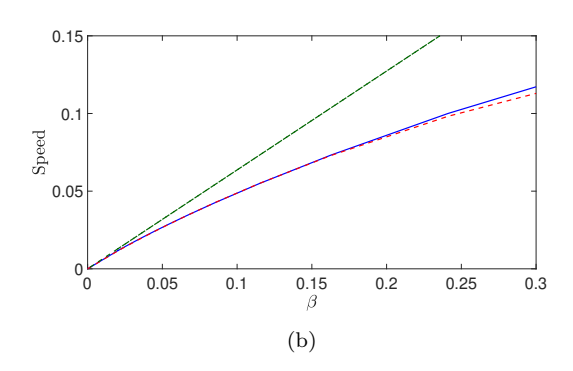


Figure 3.1. (a) Comparisons of leading-order average drift speed prediction from theory (red) with drift speed from numerical continuation (blue) for a cluster of total mass 1; see section 5 for details. (b) Numerically computed values for the drift speed (blue) plotted against the leading-order approximation (green) and the approximation with the  $\beta^{\frac{3}{2}}$  correction.

We write the center manifold as the graph of  $h^c = h^c(\alpha_+, \alpha_-, \alpha_m, p, \beta)$ , with

$$h^{c}(\alpha_{+}, \alpha_{-}, \alpha_{m}, p, \beta) = P_{n}^{*} + p + \alpha_{+}e_{+} + \alpha_{-}e_{-} + \alpha_{m}e_{n} + \mathcal{O}(|\alpha_{+}|^{2} + |\alpha_{-}|^{2} + |\alpha_{m}|^{2} + |p|^{2} + \beta^{2}).$$

In these coordinates, we have

$$\dot{P}_c = \mathcal{P}^c(f(P_n^* P_c + h^c(P_c))) + \mathcal{O}(|P_c|^3 + \beta^3),$$

where the spectral projection  $\mathcal{P}^c$  onto  $\ker Df(P_{\alpha,n}^*)$  is given by

$$\mathcal{P}^{c}v = \langle v, e_{+}^{*} \rangle e_{+} + \langle v, e_{-}^{*} \rangle e_{-} + \langle v, e_{m}^{*} \rangle e_{n} + \sum_{|i| > 3} \langle v, e_{i} \rangle e_{i}.$$

Writing the vector field in terms of  $\alpha_+, \alpha_-, \alpha_m, p, \beta$ , we find that

$$f(P_n^* + P_c + h(P_c)) = \begin{pmatrix} \vdots \\ 2p_{-3}p_{-5} - p_{-4}p_{-6} \\ -p_{-3}\alpha_{-} - p_{-3}p_{-5} \\ -h_{-} + 2p_{-3}\alpha_{-} \\ 2h_{-}\alpha_{-}\alpha_{+} - \alpha_{-}p_{-3} + \beta(1 + 2(\alpha_{m} - \alpha_{-} - \alpha_{+})) \\ 2\alpha_{+}\alpha_{-} - (h_{-} + h_{+}) - \beta(1 + 2(\alpha_{m} - \alpha_{-} - \alpha_{+})) \\ 2h_{+} - \alpha_{+}\alpha_{-} - \alpha_{+}p_{3} \\ -h_{+} + 2\alpha_{+}p_{3} \\ -\alpha_{+}p_{3} - p_{3}p_{5} \\ 2p_{3}p_{5} - p_{4}p_{6} \\ \vdots \end{pmatrix} \leftarrow +\mathcal{O}(|P_{c} + \beta|^{3})$$

which in turn gives

$$\begin{split} \dot{\alpha}_{-} &= \langle f(P_n^* + P_c + h^c(P_c)), e_-^* \rangle &= \beta - \alpha_- \alpha_+ + 3p_{-3}\alpha_- + 2\beta(\alpha_m - \alpha_+ - \alpha_-) + \mathcal{O}(3), \\ \dot{\alpha}_{+} &= \langle f(P_n^* + P_c + h^c(P_c)), e_+^* \rangle &= -\alpha_- \alpha_+ + 3p_{3}\alpha_+ + \mathcal{O}(3), \\ \dot{\alpha}_m &= \langle f(P_n^* + P_c + h^c(P_c)), e_m^* \rangle &= p_{3}\alpha_+ + p_{-3}\alpha_- + \mathcal{O}(3), \\ \dot{p}_3 &= \langle f(P_n^* + P_c + h^c(P_c)), e_3 \rangle &= -p_{3}\alpha_+ - p_{3}p_{5} + \mathcal{O}(3), \\ \dot{p}_{-3} &= \langle f(P_n^* + P_c + h^c(P_c)), e_{-3} \rangle &= -p_{-3}\alpha_- - p_{-3}p_{-5} + \mathcal{O}(3), \\ \dot{p}_4 &= \langle f(P_n^* + P_c + h^c(P_c)), e_4 \rangle &= -2p_{3}p_{5} - p_{4}p_{6} + \mathcal{O}(3), \\ \dot{p}_{-4} &= \langle f(P_n^* + P_c + h^c(P_c)), e_{-4} \rangle &= -2p_{-3}p_{-5} - p_{-4}p_{-6} + \mathcal{O}(3), \\ \dot{p}_j &= 2p_{j-1}p_{j+1} - p_j(p_{j+2} + p_{j-2}) + \mathcal{O}(3), \quad |j| > 4. \end{split}$$

At leading order, the subspace where  $p_j = 0$  for all j and  $\alpha_m = 0$  is invariant, and we therefore consider the leading-order equation for  $\alpha_-, \alpha_+$  only,

$$\dot{\alpha}_{-} = \beta - \alpha_{-}\alpha_{+} - 2\beta(\alpha_{+} + \alpha_{-}), \qquad \dot{\alpha}_{+} = -\alpha_{-}\alpha_{+}.$$

Changing variables  $x = \alpha_- + \alpha_+$  and  $\mu = \alpha_- - \alpha_+$ , this gives

$$\dot{x} = -\frac{1}{2}(x^2 - \mu^2) + \beta(1 - 2x), \qquad \dot{\mu} = \beta(1 - 2x).$$

In the natural scaling  $x \sim \mu \sim \beta^{1/2}$ , the terms  $-2\beta x$  are of higher order. The remaining terms describe precisely the slow passage through a transcritical bifurcation as studied, for instance, in [28] using geometric desingularization.

The passage near the one-site cluster can be analyzed by starting in a section to the flow  $\{x - \mu = 2\delta\}$  near  $x = -\mu = \delta$  and tracking time until the section  $x + \mu = 2\delta$  near  $x = \mu = \delta$ . At leading order this time is given by  $2\delta/\beta$ , which confirms that, at leading order, the passage time near the one-site equilibrium can be ignored in the computation of the average speed, letting, for instance,  $\delta \to 0$ . The scaling does, however, introduce error terms involving  $\beta^{1/2}$ , which indeed manifest themselves in corrections to the averaged speed of order  $\beta^{3/2}$ ; see, for instance, [28]. We did not attempt to derive these corrections analytically but numerically found the coefficient to the  $\beta^{3/2}$  correction as -.467; see Figure 3.1(b) for numerical values of the drift speed of a cluster of mass 1, plotted against the theoretical prediction with and without the  $\beta^{3/2}$  correction.

**4. Large bias regime.** In this section, we investigate the dynamics as  $\beta$  gets large. Numerically, we see that the background mass of profiles increases and that as  $\beta$  approaches 2 the size of the profiles becomes arbitrarily small relative to the background mass.

We can see that this agrees with heuristics from the spectrum of the linearization at the background mass. We recall the dispersion relation for the linearization at the uniform steady state  $u \equiv m$ ,

$$-i\omega = m(-2\cos(2\sigma) + (4+2\beta)\cos(\sigma) - (2+2\beta) + 2i\beta\sin(\sigma)),$$

and note that the quantity  $-i\omega$  has nonpositive real part exactly when  $\beta \geq 2$ . Therefore, the uniform steady state regains (marginal) linear stability when  $\beta = 2$ , which may explain

why traveling profiles disappear. For  $\beta < 2$  but sufficiently close, numerically we see small-amplitude, long-wavelength profiles atop the background state  $u \equiv m$ . In this section, we rigorously establish the existence of these spike solutions for  $\beta$  sufficiently close to 2. We first derive formal amplitude equations, giving heuristics for the existence of spike solutions. We then establish existence rigorously and derive expansions through a nonlocal center manifold computation, followed by a Melnikov analysis of the reduced system.

Formal derivation of amplitude equations. We derive formal amplitude equations for the  $\beta \sim 2$  regime, under long-wavelength, small-amplitude assumptions. We will see in section 4.2 that rigorous center manifold calculations in fact agree with the resulting amplitude equations. For our approximation, we follow [37] by choosing the regime in which the lattice spacing remains constant but the spatial variable in the KdV equation is rescaled.

Assume that (2.2) permits a small, long-wavelength solution  $P_n = m + \varepsilon^2 u(\varepsilon(n+ct), \varepsilon^3 t)$ , where  $c = 2m\beta$  is chosen as the group velocity at the constant state. To simplify notation, let  $\xi \equiv n + ct$ . Substituting the ansatz into (2.2) and grouping linear and nonlinear terms, we find

$$\begin{split} (4.1) \\ \partial_t [u(\varepsilon\xi,\varepsilon^3t)] \\ &= 2m[u(\varepsilon\xi-\varepsilon,\varepsilon^3t)+u(\varepsilon\xi+\varepsilon,\varepsilon^3t)] - m[2u(\varepsilon\xi,\varepsilon^3t)+u(\varepsilon\xi-2\varepsilon,\varepsilon^3t)+u(\varepsilon\xi+2\varepsilon,\varepsilon^3t)] \\ &+ 2m\beta\left[u(\varepsilon\xi+\varepsilon,\varepsilon^3t)-u(\varepsilon\xi,\varepsilon^3t)\right] - \varepsilon^2u(\varepsilon\xi,\varepsilon^3t)[u(\varepsilon\xi-2\varepsilon,\varepsilon^3t)+u(\varepsilon\xi+2\varepsilon,\varepsilon^3t)] \\ &+ 2\varepsilon^2u(\varepsilon\xi-\varepsilon,\varepsilon^3t)u(\varepsilon\xi+\varepsilon,\varepsilon^3t) + \beta\varepsilon^2\left[u^2(\varepsilon\xi+\varepsilon,\varepsilon^3t)-u^2(\varepsilon\xi,\varepsilon^3t)\right]. \end{split}$$

We now expand u in the first variable,

$$u(\varepsilon\xi + k\varepsilon, \varepsilon^{3}t) = u(\varepsilon\xi, \varepsilon^{3}t) + k\varepsilon \cdot \partial_{1}u(\varepsilon\xi, \varepsilon^{3}t) + \frac{(k\varepsilon)^{2}}{2!} \cdot \partial_{1}^{2}u(\varepsilon\xi, \varepsilon^{3}t) + \frac{(k\varepsilon)^{3}}{3!} \cdot \partial_{1}^{3}u(\varepsilon\xi, \varepsilon^{3}t) + \frac{(k\varepsilon)^{4}}{4!} \cdot \partial_{1}^{4}u(\varepsilon\xi, \varepsilon^{3}t) + \mathcal{O}(\varepsilon^{5}),$$

for each  $k \in \{-2, -1, 0, 1, 2\}$ , and we implicitly assume sufficient smoothness in u. Inserting the expansion into (4.1), we find

$$\begin{split} \varepsilon^{3}\partial_{2}u &= 2m\left[\varepsilon^{2}\partial_{1}^{2}u + \frac{\varepsilon^{4}}{12}\partial_{1}^{4}u\right] - m\left[4\varepsilon^{2}\partial_{1}^{2}u + \frac{4}{3}\varepsilon^{4}\partial_{1}^{4}u\right] + 2m\beta\left[\frac{\varepsilon^{2}}{2}\partial_{1}^{2}u + \frac{\varepsilon^{3}}{6}\partial_{1}^{3}u + \frac{\varepsilon^{4}}{24}\partial_{1}^{4}u\right] \\ &- \varepsilon^{2}\left[2u^{2} + 4\varepsilon^{2}u\partial_{1}^{2}u + \frac{4\varepsilon^{4}}{3}u\partial_{1}^{4}u\right] \\ &+ 2\varepsilon^{2}\left[u^{2} + \varepsilon^{2}u\partial_{1}^{2}u - \varepsilon^{2}(\partial_{1}u)^{2} + \frac{\varepsilon^{4}}{12}u\partial_{1}^{4}u - \frac{\varepsilon^{4}}{3}\partial_{1}u\partial_{1}^{3}u + \frac{\varepsilon^{4}}{4}(\partial_{1}^{2}u)^{2}\right] \\ &+ \beta\varepsilon^{2}\left[2\varepsilon u\partial_{1}u + \varepsilon^{2}u\partial_{1}^{2}u + \varepsilon^{2}(\partial_{1}u)^{2} + \varepsilon^{3}\partial_{1}u\partial_{1}^{2}u + \frac{\varepsilon^{3}}{3}u\partial_{1}^{3}u + \frac{\varepsilon^{4}}{4}(\partial_{1}^{2}u)^{2} \right. \\ &+ \frac{\varepsilon^{4}}{12}u\partial_{1}^{4}u + \frac{\varepsilon^{4}}{3}\partial_{1}u\partial_{1}^{3}u\right] \\ &+ \mathcal{O}(\varepsilon^{5}), \end{split}$$

where  $\partial_1$  and  $\partial_2$  refer to the partial derivatives with respect to the first and second arguments  $\varepsilon \xi$  and  $\varepsilon^3 t$ , respectively. Retaining orders  $\mathcal{O}(\varepsilon^2)$  to  $\mathcal{O}(\varepsilon^4)$  and then dividing by  $\varepsilon^3$ , we find the formal amplitude equation

$$\partial_{2}u = \frac{m(\beta - 2)}{\varepsilon}\partial_{1}^{2}u + \frac{m\beta}{3}\partial_{1}^{3}u + 2\beta u\partial_{1}u - \varepsilon\left(\frac{(14 - \beta)m}{12}\partial_{1}^{4}u + (2 - \beta)\partial_{1}(u\partial_{1}u)\right) + \mathcal{O}(\varepsilon^{2}).$$

Note that for  $\beta = 2 + \mathcal{O}(\varepsilon^2)$ , at leading order, (4.2) becomes the KdV equation

(4.3) 
$$\partial_2 u = \frac{2m}{3} \partial_1^3 u + 4u \partial_1 u.$$

The KdV equation possesses a family of traveling spikes parameterized by the wave speed (or the amplitude). At the next order  $\mathcal{O}(\varepsilon)$ , with  $\beta=2-\varepsilon^2\tilde{\beta}$ ,  $\tilde{\beta}>0$ , we find a damping term  $-\varepsilon m\partial_1^4 u$ , fourth-order viscosity and a negative damping term  $-\varepsilon m\tilde{\beta}\partial_1^2 u$ , negative viscosity. The analysis presented below demonstrates that this equation can be rigorously derived as an ODE at leading order on a center manifold and that the effects of negative and positive viscosity balance for an appropriate wave speed (or amplitude) in the reduced center manifold equation.

Remark 4.1 (viscous Burgers modulation and stability). For  $\beta > 2$ , one finds that (4.2) reduces at leading order to the viscous Burgers equation,  $\partial_2 u = \partial_1^2 u + u \partial_1 u$ , after appropriate scalings. It is known that in this approximation, localized initial conditions decay algebraically in  $L^{\infty}$  and that higher-order terms, that is, terms carrying higher powers in u or more derivatives, are irrelevant in the long-time asymptotics of small data; see [8]. We therefore suspect that one can establish asymptotic stability in  $\ell^{\infty}$  of constant distributions of opinions in our system for values of  $\beta > 2$  and small perturbations in  $\ell^1$ . On the other hand,  $\ell^{\infty}$  perturbations may evolve into persistent dynamics, for instance viscous shocks, rarefaction waves, and their superposition; see [13] for such a construction based on a Burgers approximation.

**4.1. Statement of main result.** In order to precisely state the main result of this section, we collect some definitions and notation. We define a traveling wave in a one-dimensional lattice as a solution of the form  $P_n = Q(n+ct)$ , where  $Q(\cdot)$  defines a fixed profile which moves through the lattice. Seeking such a solution, we reformulate the problem as a functional differential equation: substituting  $P_n = Q(n+ct)$ , we get

$$(4.4) 0 = -cQ'(\xi) + 2Q(\xi - 1)Q(\xi + 1) - Q(\xi)(Q(\xi - 2) + Q(\xi + 2)) + \beta(Q^{2}(\xi + 1) - Q^{2}(\xi)),$$

where  $\xi = n + ct \in \mathbb{R}$ .

Further writing  $Q(\xi) = m + q(\xi)$ , we have

$$(4.5) 0 = -cq'(\xi) + m(2q(\xi - 1) + 2(\beta + 1)q(\xi + 1) - 2(\beta + 1)q(\xi) - q(\xi - 2) - q(\xi + 2) + \mathcal{N}(q, \beta)),$$

where 
$$\mathcal{N}(q,\beta) = 2q(\xi-1)q(\xi+1) - q(\xi)(q(\xi-2) + q(\xi+2)) + \beta(q(\xi+1)^2 - q(\xi)^2).$$

Note that we can rewrite the forward-backward delay equation (4.5) as a nonlocal equation

$$(4.6) 0 = -cq'(\xi) - 2m(\beta + 1)q(\xi) + m\mathcal{K} * q + \mathcal{N}(q, \beta),$$

with convolution kernel  $\mathcal{K}(\cdot) = -\delta(\cdot - 2) + 2\delta(\cdot - 1) + 2(\beta + 1)\delta(\cdot + 1) - \delta(\cdot + 2)$ .

We are now ready to state the main result of this section.

Theorem 1. There exists  $\beta_* > 0$  such that for  $2 - \beta_* < \beta < 2$ , there exists a locally unique homoclinic solution  $q = q_{\beta}^*(\xi)$  to (4.6) with locally unique wave speed  $c = c(\beta)$ , with  $\lim_{|\xi| \to \infty} q_{\beta}^*(\xi) = m$ , and therefore a unique traveling-wave spike solution  $(u_{\beta}^*)_n(t) = q_{\beta}^*(n+ct)$  to (2.2). Furthermore, we have

$$q_{\beta}^{*}(\xi) = m \left( 1 + \frac{7(2-\beta)}{10} \right) \operatorname{sech}^{2} \left( \sqrt{\frac{7(2-\beta)}{20}} \xi \right) + \mathcal{O}((2-\beta)^{\frac{3}{2}}),$$

$$c(\beta) = m \left( 4 - \frac{16}{15} (2-\beta) \right) + \mathcal{O}((2-\beta)^{\frac{3}{2}}).$$

Note that, in particular,  $q_{\beta}^*(\xi) > m$  represents an opinion spike, or a traveling cluster, and  $c = c(\beta) > 2m\beta$  is slightly larger than the linear group velocity  $2m\beta$ .

The outline of the proof is as follows: We first show that (4.6) can be reformulated to satisfy the hypotheses of the nonlocal center manifold theorem in [16], allowing for a center manifold reduction. We then calculate the nonlocal center manifold expansion in function space and derive the reduced vector field. Finally, we prove the existence of homoclinic solutions to the reduced equations using Melnikov analysis, where the existence of a conserved quantity becomes crucial.

We begin with the existence of a center manifold. Let  $\tilde{\beta} = 2 - \beta$ ,  $\tilde{c} = c - 4m$ , and define

$$\mathcal{T}_{\tilde{\beta},\tilde{c}}q = -cq' - 2m(3 - \tilde{\beta})q + m\mathcal{K} * q$$

as an operator on  $H^1_{-\eta}(\mathbb{R},\mathbb{R})$  where

$$||u||_{H^1_{-\eta}} = ||u(\cdot)e^{-\eta|\cdot|}||_{H^1}$$

is an exponentially weighted space allowing for exponential growth. For  $\eta > 0$  sufficiently small, consider the kernel  $\mathcal{E}_0$ , which turns out to be finite-dimensional, and choose a closed complement, thus defining a projection  $\mathcal{P}_0$  onto the kernel  $\mathcal{P}_0$ ,

$$\mathcal{E}_0 = \ker \mathcal{T}_{0,0}, \qquad \mathcal{P}_0 \mathcal{E}_0 = \mathcal{E}_0.$$

Proposition 4.2. Fix  $\eta > 0$  sufficiently small, and consider the functional equation (4.6) in  $H^1_{-\eta}(\mathbb{R},\mathbb{R})$  and  $k < \infty$ . There exist neighborhoods  $\mathcal{U}_q \times \mathcal{U}_{(0,0)}$  of (0,0,0) in  $\mathcal{E}_0 \times \mathbb{R}^2$  and a map  $\Psi \in \mathcal{C}^k(\mathcal{U}_q \times \mathcal{U}_{(0,0)}, \ker \mathcal{P}_0)$ , with  $\Psi(0,0,0) = 0$  and  $D_q\Psi(0,0,0) = 0$  such that for all  $(\tilde{\beta}, \tilde{c}) \in \mathcal{U}_{(0,0)}$  the manifold

$$\mathcal{M}_0^{\tilde{\beta},\tilde{c}} = \left\{ q_0 + \Psi(q_0, \tilde{\beta}, \tilde{c}) : q_0 \in \mathcal{U}_q, \right\} \subset H^1_{-\eta}$$

contains the set of all bounded solutions of (4.6), small in  $C^0(\mathbb{R}, \mathbb{R})$ .

*Proof.* Preconditioning (4.6) with the operator  $\left(2m(\beta+1)+c\frac{d}{d\xi}\right)^{-1}=G_{\beta,c}*$ , with

$$G_{\beta,c}(\xi) = \frac{1}{c} \exp\left(-\frac{2m(\beta+1)}{c}\xi\right) \chi_{\mathbb{R}^+}(\xi),$$

the resulting equation

(4.7) 
$$0 = -q + (G_{\beta,c} * m\mathcal{K}) * q + G_{\beta,c} * \mathcal{N}(q,\beta)$$
$$= : -q + \widetilde{\mathcal{K}}_{\beta,c} * q + \widetilde{\mathcal{N}}(q,\beta)$$

is in the form of [16], with one discrepancy—the kernel  $\widetilde{\mathcal{K}}_{\beta,c} = G_{\beta,c} * m\mathcal{K}$  is not in  $W_{\eta_0}^{1,1}$  for any  $\eta_0 > 0$ . However, since  $\widetilde{\mathcal{K}}'_{\beta,c}$  is still a sum of an  $L^1_{\eta_0}$  function and scaled translates of Dirac deltas, the results of [16] can be established with minor modifications as follows. In the proof of [16, Lemma 3.1], the smoothness of  $\mathcal{K}$  is only used to show that  $\mathcal{DT}(u) = \mathcal{D}(\mathcal{K} * u) = (\mathcal{K}' + \rho \mathcal{K} + \rho \delta_0) * u$  satisfies the hypotheses of [15]. Here, we note that although  $\widetilde{\mathcal{K}}_{\beta,c} \notin W_{\eta_0}^{1,1}$ , it is still true that  $(\widetilde{\mathcal{K}}'_{\beta,c} + \rho \widetilde{\mathcal{K}}_{\beta,c} + \rho \delta_0) * u$  satisfies the hypotheses of [15]. Therefore, [16, Lemma 3.1] holds identically, and the rest of the proof in [16] does not use this hypothesis. The parameter-dependent center manifold theorem [16, Theorem 3] can therefore be applied to the system (4.6), which implies the statement of the proposition.

**4.2.** Nonlocal center manifold expansion. Given the existence of a nonlocal center manifold, we now use the methods of [16] to calculate the Taylor expansion of the center manifold in function space and derive the reduced vector field.

Since the Taylor expansion is written as a map over the kernel of  $\mathcal{T}_{\tilde{\beta},\tilde{c}}$ , we first find a parameterization of ker  $\mathcal{T}_{\tilde{\beta},\tilde{c}}$ , and a projection. The dispersion relation given by the linearized equation, in terms of  $\tilde{\beta},\tilde{c}$ , is

$$d(\nu, \tilde{\beta}, \tilde{c}) = \widehat{\mathcal{T}_{\tilde{\beta}, \tilde{c}}}(\nu) = -(4m + \tilde{c})\nu - 2m(3 + \tilde{\beta}) + 2m(e^{\nu} + e^{-\nu}) - 2m(e^{2\nu} + e^{-2\nu}) + 2m(2 - \tilde{\beta})e^{\nu} = 0.$$

Note that d is clearly analytic and roots on the imaginary axis  $\nu \in i\mathbb{R}$  are a priori bounded. At  $\tilde{\beta} = \tilde{c} = 0$ , we find that there are no imaginary roots  $\nu \neq 0$ . Expanding d at  $\nu = 0$ , we have

$$d(\nu, \tilde{\beta}, \tilde{c}) = (2m\tilde{\beta} - \tilde{c})\nu + m\tilde{\beta}\nu^2 + \frac{m(2 - \tilde{\beta})}{3}\nu^3 - \frac{m(\tilde{\beta} + 12)}{12}\nu^4 + \mathcal{O}(\nu^5).$$

Note that  $\widetilde{d}(0,0,0) = \partial_{\nu}\widetilde{d}(0,0,0) = \partial_{\nu\nu}\widetilde{d}(0,0,0) = 0$ , with  $\partial_{\nu\nu\nu}\widetilde{d}(0,0,0) \neq 0$ . Additionally,  $\widetilde{d}(i\ell,0,0) \neq 0$  for all  $\ell \neq 0$ . Thus, the kernel  $\mathcal{E}_0$  of  $\mathcal{T}_{0,0}$  in  $H^1_{-n}$  is given by

$$\mathcal{E}_0 = \operatorname{span}\{1, \xi, \xi^2\},\,$$

and we write elements  $q_0 \in \mathcal{E}_0$  as

$$(4.8) q_0(\xi) = A_0 + A_1 \xi + A_2 \xi^2 \in \mathcal{E}_0,$$

with  $(A_0, A_1, A_2) \in \mathbb{R}^3$ . Last, we define the projection  $\mathcal{P}_0 : H^3_{-\nu}(\mathbb{R}) \to \mathcal{E}_0$  by

$$\mathcal{P}_0(q) = q_0 + q'(0)\xi + \frac{1}{2}q''(0)\xi^2,$$

noting that this is well-defined by Sobolev embedding and using that the solutions are actually in  $H^k$  for k as in the statement of Proposition 4.2.

The calculation of a reduced center flow is done in two steps: first, invariance is used to derive a Taylor expansion for the nonlocal center manifold  $\Psi$  from Proposition 4.2. Second,

the flow  $\Phi_{\eta}$  on the center manifold, which is defined by the action of translations  $\xi \mapsto \xi + \eta$  on  $H^1_{-\eta}$ , is projected onto the kernel and differentiated with respect to  $\eta$  at  $\eta = 0$ , yielding a finite-dimensional reduced vector field. We note that the bulk of the computation in this process is in the first step since the second step will consist entirely of differentiating polynomials. In fact, the entire computation involves only polynomials, highlighting the algebraic simplicity of the method.

In writing the center manifold as a graph  $\Psi$  over  $\mathcal{E}_0$ , we seek a Taylor expansion of the form

(4.9) 
$$\Psi(A_0, A_1, A_2, \tilde{\beta}, \tilde{c}) = \sum_{\substack{l,r\\|l|+|r|>1}} A_0^{l_0} A_1^{l_1} A_2^{l_2} \tilde{\beta}^{r_1} \tilde{c}^{r_2} \psi_{l,r}(\xi),$$

where  $l = (l_1, l_2, l_3), r = (r_1, r_2)$ . Here, the second multi-index r is present because we are using the parameter-dependent version of [16, Theorem 1]. We will use invariance to solve for the Taylor coefficients  $\psi_{l,r}$ . Note that we do this using the unconditioned equation (4.6) since it makes calculations more straightforward and yields identical results. We substitute (4.9) into the functional differential equation (4.6), noting that

$$(4.10) \ \mathcal{T}_{\tilde{\beta}\,\tilde{c}}(q_0 + \Psi) + \mathcal{N}(q_0 + \Psi) = -\tilde{c}q_0'(\xi) - 2m\tilde{\beta}(q_0(\xi + 1) - q_0(\xi)) + \mathcal{N}(q_0, 0) + \mathcal{T}_{0,0}(\Psi) + \mathcal{O}(3),$$

to obtain at quadratic order that

$$(4.11) \sum_{\substack{|l|+|r|=2}} A_0^{l_0} A_1^{l_1} A_2^{l_2} \tilde{\beta}^{r_1} \tilde{c}^{r_2} \mathcal{T}_{0,0}(\psi_{l_0,l_1,l_2,r_1,r_2}(\xi)) = \tilde{c} q_0'(\xi) + 2m \tilde{\beta}(q_0(\xi+1) + q_0(\xi)) - \mathcal{N}(q_0,0)$$

$$= 4A_0 A_1 + 4\xi A_1^2 + 8\xi A_0 A_2 + (12\xi^2 + 4)A_1 A_2 + (8\xi^3 + 8\xi + 4)A_2^2$$

$$- 2m A_1 \tilde{\beta} - A_1 \tilde{c} + (-2m - 4m\xi)A_2 \tilde{\beta} - 2\xi A_2 \tilde{c}.$$

We then take as an ansatz for  $\psi_{l,r}$  the polynomials  $\psi_{l,r} = \sum_{i \geq 3} \alpha_i \xi^i$ , suppressing the dependence on l,r in  $\alpha_i$ . The ansatz is inspired by the fact that the kernel  $\mathcal{E}_0$  consists of polynomials and more generally that the space of polynomials is invariant under convolution. We calculate

$$\mathcal{T}_{0,0}(\alpha_3\xi^3 + \alpha_4\xi^4 + \alpha_5\xi^5 + \alpha_6\xi^6) = (4m)\alpha_3 + (16m\xi - 24m)\alpha_4 + (40m\xi^2 - 120m\xi + 4m)\alpha_5 + (80\xi^3 - 360m\xi^2 + 24m\xi - 120m)\alpha_6$$

and compare coefficients between (4.12) and (4.11) for each quadratic power of  $(A_0, A_1, A_2, \tilde{\beta}, \tilde{c})$ . After doing so, one finds that the nonzero Taylor coefficients at quadratic order are

$$\begin{split} & (4.13) \\ & \psi_{1,1,0,0,0} = -\frac{1}{m} \xi^3, \quad \psi_{0,2,0,0,0} = -\frac{1}{4m} \xi^4 - \frac{3}{2m} \xi^3, \quad \psi_{1,0,1,0,0} = -\frac{1}{2m} \xi^4 - \frac{3}{m} \xi^3, \\ & \psi_{0,1,1,0,0} = -\frac{3}{10m} \xi^5 - \frac{9}{4m} \xi^4 - \frac{71}{5m} \xi^3, \quad \psi_{0,0,2,0,0} = -\frac{1}{10m} \xi^6 - \frac{9}{10m} \xi^5 - \frac{71}{10m} \xi^4 - \frac{457}{10m} \xi^3, \\ & \psi_{0,1,0,1,0} = \frac{1}{2} \xi^3, \quad \psi_{0,1,0,0,1} = \frac{1}{4m} \xi^3, \quad \psi_{0,0,1,1,0} = \frac{1}{4} \xi^4 + 2 \xi^3, \quad \psi_{0,0,1,0,1} = \frac{1}{8m} \xi^4 + \frac{3}{4m} \xi^3. \end{split}$$

We can now compute the reduced vector field on the center manifold. We start by noting that the flow on the center manifold is defined by the action of translations, that is, at finite order,

(4.14) 
$$\Phi_{\eta}((q_0 + \Psi)(\xi)) = (q_0 + \Psi)(\xi + \eta)$$

$$= q_0(\xi + \eta) + \sum_{l=0}^{\infty} A_0^{l_0} A_1^{l_1} A_2^{l_2} \tilde{\beta}^{r_1} \tilde{c}^{r_2} \psi_{l,r}(\xi + \eta),$$

with  $q_0, \psi_{l,r}$  as in (4.11), (4.12). This flow becomes a reduced flow after projection by  $\mathcal{P}_0$  onto the kernel and last becomes a reduced vector field after differentiation at  $\eta = 0$ :

$$(4.15) q_0' = \frac{d}{d\eta} \mathcal{P}_0(\Phi_\eta(q_0 + \Psi))\Big|_{\eta=0}.$$

In order to express (4.15) in terms of  $(A_0, A_1, A_2)$ , we note that  $(q_0 + \Psi)(\xi + \eta)$  is a sum of polynomials in  $\xi + \eta$  and calculate

$$\begin{split} \frac{d}{d\eta}\mathcal{P}_0((\xi+\eta))|_{\eta=0} &= (1,0,0), \frac{d}{d\eta}\mathcal{P}_0((\xi+\eta)^2)|_{\eta=0} = (0,2,0), \frac{d}{d\eta}\mathcal{P}_0((\xi+\eta)^3)|_{\eta=0} = (0,0,3), \\ &\frac{d}{d\eta}\mathcal{P}_0((\xi+\eta)^n)|_{\eta=0} = (0,0,0), \, n \neq 1,2,3. \end{split}$$

Then, using the expressions for  $\Psi$  and  $q_0$  in (4.13) and (4.8) and gathering terms, we find the reduced vector field to be given by

$$\begin{aligned} &(4.16) \\ &\frac{dA_0}{d\eta} = A_1 + \mathcal{O}(3), \\ &\frac{dA_1}{d\eta} = 2A_2 + \mathcal{O}(3), \\ &\frac{dA_2}{d\eta} = -\frac{3}{m} \left( A_0 A_1 + \frac{3}{2} A_1^2 + 3A_0 A_2 - \frac{m}{2} A_1 \tilde{\beta} - \frac{1}{4} A_1 \tilde{c} - 2m A_2 \tilde{\beta} - \frac{3}{4} A_2 \tilde{c} + \frac{71}{5} A_1 A_2 + \frac{457}{10} A_2^2 \right) \\ &+ \mathcal{O}(3). \end{aligned}$$

4.3. Existence of solutions to reduced equations. It turns out that this three-dimensional ODE possesses a conserved quantity at leading order. Within level sets of this conserved quantity, one finds at leading order a homoclinic solution. In order to prove persistence of the homoclinic, one needs to prevent drift along level sets under perturbations of arbitrarily high order. To this aim, we establish the existence of a quantity that is *exactly* conserved, which we compute to leading order following the ideas in [2]. Within level sets of this exact conserved quantity, we then use a somewhat standard Melnikov-type argument to find homoclinics for the perturbed equation.

In order to derive a conserved quantity, we integrate (4.4) from 0 to  $L, L \in \mathbb{R}$ , and simplify to find

$$0 = -cQ(L) + \int_{L-1}^{L} Q(y-1)Q(y+1)dy - \int_{L}^{L+1} Q(y-1)Q(y+1)dy + \beta \int_{L}^{L+1} Q^{2}(y)dy - \left(-cQ(0) + \int_{-1}^{0} Q(y-1)Q(y+1)dy - \int_{0}^{1} Q(y-1)Q(y+1)dy + \beta \int_{0}^{1} Q^{2}(y)dy\right)$$

for any  $L \in \mathbb{R}$ . Hence,  $\Phi[Q]$ , defined by

$$(4.17) \quad \Phi[Q] = -cQ(0) + \int_{-1}^{0} Q(y-1)Q(y+1)dy - \int_{0}^{1} Q(y-1)Q(y+1)dy + \beta \int_{0}^{1} Q^{2}(y)dy,$$

is translation invariant on solutions, i.e.,  $\Phi[Q] = \Phi[S_{\tau}Q]$ , where  $S_{\tau}$  is a translation operator. We therefore define  $\varphi \equiv \Phi[Q]$  as the equivalent of a true conserved quantity or first integral.

Then, letting  $Q(\xi) = m + A_0 + A_1 \xi + A_2 \xi^2 + \Psi(A_0, A_1, A_2, \widetilde{\beta}, \widetilde{c})$  be an element of the center manifold, we insert Q into (4.17) to obtain

(4.18)

$$\varphi[Q] = (-2m^2 - m^2\tilde{\beta} - m\tilde{c}) + \frac{4m}{3}A_2 + 2A_0^2 - (2m\tilde{\beta} + \tilde{c})A_0 - \left(4m\tilde{\beta} + \frac{3}{2}\tilde{c}\right)A_1 + 6A_0A_1 + \frac{284}{15}A_0A_2 + \frac{142}{15}A_1^2 - \left(\frac{187m}{15}\tilde{\beta} + \frac{22}{5}\tilde{c}\right)A_2 + \frac{457}{5}A_1A_2 + \frac{50201}{175}A_2^2 + \mathcal{O}(3).$$

We see that there exists a locally invertible change of coordinates where  $A_2$  maps to  $\phi$ . We can solve (4.18) for  $A_2$  using the implicit function theorem, since  $\frac{4m}{3} \neq 0$ , to find

$$A_{2} = \frac{3}{4m}\phi + \frac{3}{4m}(2m\tilde{\beta} + \tilde{c})A_{0} - \frac{3}{2m}A_{0}^{2} - \frac{9}{2m}A_{0}A_{1} + \frac{3}{4m}\left(4m\beta + \frac{3}{2}\tilde{c}\right)A_{1} - \frac{71}{10m}A_{1}^{2}$$

$$+ \frac{99}{40m^{2}}\tilde{c}\phi + \frac{561}{80}\tilde{\beta}\phi - \frac{213}{20m^{2}}A_{0}\phi - \frac{4113}{80m^{2}}A_{1}\phi - \frac{1355427}{11200m^{3}}\phi^{2} + \mathcal{O}(3)$$

$$=: g(A_{0}, A_{1}, \phi) + \mathcal{O}(3),$$

where  $\phi$  is redefined to equal  $\varphi + 2m^2 + m^2\tilde{\beta} + m\tilde{c}$  since the latter is also conserved. We also define  $\widetilde{A}_1 = \frac{dA_0}{d\eta} = A_1 + \mathcal{O}(3)$  and note that by the implicit function theorem we can find  $A_1$  in terms of  $\widetilde{A}_1$  with an expansion. Changing coordinates to  $(A_0, \widetilde{A}_1, \phi)$ , we have the system

$$\frac{dA_0}{d\eta} = \widetilde{A}_1,$$

$$\frac{d\widetilde{A}_1}{d\eta} = 2g(A_0, \widetilde{A}_1, \phi) + \mathcal{O}(3),$$

$$\frac{d\phi}{d\eta} = 0.$$

We now rescale. Let  $\tilde{c} = \tilde{\beta}mc_0$ , and rescale the spatial variable by choosing  $\eta = (3\tilde{\beta})^{\frac{1}{2}}(1 + \frac{c_0}{2})^{\frac{1}{2}}\zeta$  and the amplitudes by  $A_0 = \tilde{\beta}m(1 + \frac{c_0}{2})a_0$ ,  $\tilde{A}_1 = \tilde{\beta}^{\frac{3}{2}}\sqrt{3}m(1 + \frac{c_0}{2})^{\frac{3}{2}}a_1$ , and  $\phi = \tilde{\beta}^2 3m^2(1 + \frac{c_0}{2})^2\tilde{\phi}$ . Substituting, we obtain the final reduced system

$$\frac{da_0}{d\zeta} = a_1, 
(4.21) \quad \frac{da_1}{d\zeta} = \frac{1}{2}\tilde{\phi} + a_0 - a_0^2 - \tilde{\beta}^{\frac{1}{2}}\sqrt{3} \left[ 3\left(1 + \frac{c_0}{2}\right)^{\frac{1}{2}} a_0 a_1 - \left(1 + \frac{c_0}{2}\right)^{-\frac{1}{2}} \left(2 + \frac{3c_0}{4}\right) a_1 \right] + \mathcal{O}(\tilde{\beta}), 
\frac{d\tilde{\phi}}{d\zeta} = 0.$$

We are looking for homoclinics to  $a_0 = 0$  since we are interested in homoclinics with background mass m. We therefore choose  $\widetilde{\phi} \equiv 0$  as a solution to the third equation, reducing to (4.22)

$$0 = a_0'' - a_0 + a_0^2 - \tilde{\beta}^{\frac{1}{2}} \sqrt{3} \left[ 3 \left( 1 + \frac{c_0}{2} \right)^{\frac{1}{2}} a_0 a_0' - \left( 1 + \frac{c_0}{2} \right)^{-\frac{1}{2}} \left( 2 + \frac{3c_0}{4} \right) a_0' \right] + \mathcal{O}(\tilde{\beta}) =: F(a_0, \tilde{\beta}),$$

where  $' = \partial_{\zeta}$ . Note that for  $\tilde{\beta} = 0$ , this equation admits the explicit homoclinic solution  $a_*(\zeta) = \frac{3}{2} \operatorname{sech}^2(\frac{\zeta}{2})$ .

We now prove the existence of homoclinic solutions to (4.22) using a standard Melnikov analysis.

Lemma 4.3. There exists  $\tilde{\beta}_* > 0$  such that for  $0 < \tilde{\beta} < \tilde{\beta}_*$ , (4.22) admits a homoclinic solution to  $a_0 = 0$  that is uniformly  $\mathcal{O}(\tilde{\beta}^{1/2})$ -close to  $a_*(\zeta)$ .

*Proof.* Let  $a_*(\zeta)$  be as above. Linearizing (4.22) at  $a_0 = a_*, \tilde{\beta} = 0$  yields the linear operator

$$\mathcal{L}_* u = \partial_{\zeta\zeta} u + 2a_* u - u.$$

We note that  $\ker \mathcal{L}_* = \operatorname{span}\{a'_*\}$ . Define the projection  $\mathcal{P}$  onto  $\ker \mathcal{L}^*$  by  $\mathcal{P}u = \langle a'_*, u \rangle$ , where  $\langle \cdot, \cdot \rangle$  denotes the  $L^2$ -inner product over  $\mathbb{R}$ . Note also that  $\mathcal{L}_*$  is a self-adjoint operator. Then, writing  $a_0 = a_* + v + \alpha a'_*$ , where  $v \in (\ker \mathcal{L}_*)^{\perp}$ , we wish to solve  $F(a_* + v + \alpha a'_*, \tilde{\beta}) = 0$ . Without loss of generality, we fix a translate of any potential solution by choosing  $\alpha = 0$ , arriving at

(4.23) 
$$0 = \mathcal{P}F(a_* + v, \tilde{\beta}),$$
$$0 = (1 - \mathcal{P})F(a_* + v, \tilde{\beta}).$$

By the implicit function theorem, since the linearization  $(1 - \mathcal{P})DF(a_*, \tilde{\beta}) = (1 - \mathcal{P})\mathcal{L}_*$  is invertible as an operator from  $\ker \mathcal{L}^{\perp}$  to  $\operatorname{Ran} \mathcal{L}$ , there exists a smooth function  $v = \psi(\tilde{\beta})$  defined on a neighborhood of 0 such that  $(1 - \mathcal{P})F(a_* + \psi(\tilde{\beta}), \tilde{\beta}) = 0$ . Inserting  $\psi$  into the first equation, we get the reduced equation

(4.24)

$$0 = \mathcal{P}F(a_* + \psi(\tilde{\beta}), \tilde{\beta})$$

$$= \langle a'_*, \mathcal{L}_* \psi(v) \rangle + \tilde{\beta}^{\frac{1}{2}} \sqrt{3} \left[ 3 \left( 1 + \frac{c_0}{2} \right)^{\frac{1}{2}} \langle a'_*, a_* a'_* \rangle - \left( 1 + \frac{c_0}{2} \right)^{-\frac{1}{2}} \left( 2 + \frac{3c_0}{4} \right) \langle a'_*, a'_* \rangle \right] + \mathcal{O}(\tilde{\beta}).$$

Noting that  $\langle a'_*, \mathcal{L}_*\psi(v)\rangle = \langle \mathcal{L}_*a'_*, \psi(v)\rangle = 0$ , and dividing by  $\tilde{\beta}^{\frac{1}{2}}$ , we get

$$(4.25) 0 = 3\left(1 + \frac{c_0}{2}\right)\langle a'_*, a_*a'_* \rangle - \left(2 + \frac{3c_0}{4}\right)\langle a'_*, a'_* \rangle + \mathcal{O}\left(\tilde{\beta}^{\frac{1}{2}}\right).$$

At  $\tilde{\beta} = 0$ , we can explicitly find that  $c_0 = \frac{4\langle a'_*, a'_* \rangle}{3\langle a''_*, a''_* \rangle} - 2 = -\frac{16}{15}$ . Noting that (4.25) is smooth in  $\delta = \tilde{\beta}^{\frac{1}{2}}$ , there exists  $c_0 = c_0(\delta)$  for  $|\delta| < \delta_*$ , by the implicit function theorem, since  $\frac{\partial}{\partial c_0} \mathcal{P}F = \frac{3}{4}\langle a''_*, a''_* \rangle = \frac{18}{7} \neq 0$ , such that (4.25) is satisfied.

Then for  $0 < \tilde{\beta} < \tilde{\beta}_* := \delta_*^2$  there exists a solution to (4.22), with the scaled correction  $c_0$  to the speed given by

$$c_0(\beta) = -\frac{16}{15} + \mathcal{O}(\tilde{\beta}^{\frac{1}{2}}).$$

Putting this together, we see that Theorem 1 is proven, and we have that a homoclinic solution to the system (4.16) exists for  $\beta \leq 2$ , with the speed parameter given by

$$c(\beta) = m(4 - c_0\tilde{\beta}) + \mathcal{O}(\tilde{\beta}^{\frac{3}{2}}) = \frac{4m}{15} (7 + 4\beta) + \mathcal{O}((2 - \beta)^{\frac{3}{2}}).$$

- 5. Cluster drift: Numerical continuation and stability. We explore the existence and stability of traveling clusters numerically for  $0 < \beta < 2$ . The numerical results connect the two asymptotics regimes  $\beta \gtrsim 0$  (section 3) and  $\beta \lesssim 2$  (section 4). In particular, the results confirm the asymptotics and existence results with good quantitative agreement and provide a more global picture of drift in the parameter  $\beta$ . In addition to these numerical continuation studies, we present a glimpse into the intricate question of stability and selection: instabilities in the constant cluster tails grow and lead to the formation of new clusters.
- **5.1. Connecting the regimes—secant continuation.** We compute traveling profiles throughout the entire range  $0 < \beta < 2$  using a Newton method to find fixed points of the functional equation (4.5),

$$0 = -cq'(\xi) + m(2q(\xi - 1) + 2(\beta + 1)q(\xi + 1) - 2(\beta + 1)q(\xi) - q(\xi - 2) - q(\xi + 2) + \mathcal{N}(q, \beta)), \qquad \xi \in \mathbb{R}.$$

We truncate the real line  $\xi \in \mathbb{R}$  to  $\xi \in [-L/2, L/2]$  and impose (artificial) periodic boundary conditions. We then discretize (5.1) with N points and a grid spacing  $h = L/N = 1/\ell$ ,  $\ell \in \mathbb{N}$ , so that shifted values can be evaluated on the grid, using a fourth-order finite difference approximation for the derivative.

The linearization at a given profile  $q_*$  possesses a two-dimensional generalized kernel, at least, generated by  $q'_*$  from translations and by  $q_*$  from mass scaling. We therefore add the following constraints:  $\int \xi q_* = 0$  eliminates translations, and  $\int q_* = M$  fixes the mass. We compensate for the lack of a Lagrange multiplier associated with the mass constraint through the introduction of a dummy mass loss term  $\mu q(\xi)$ . In summary, we solve the system

(5.2) 
$$-cq'(\xi) + m[2q(\xi - 1) + 2(\beta + 1)(q(\xi + 1) - q(\xi)) - q(\xi - 2) - q(\xi + 2) + \mathcal{N}(q, \beta)]$$
$$+ \mu q = 0, \quad \xi \in \left[ -\frac{L}{2}, \frac{L}{2} \right],$$

(5.3) 
$$\int_{-L/2}^{L/2} \xi q(\xi) d\xi = 0,$$

(5.4) 
$$\int_{-L/2}^{L/2} (q(\xi) - m) d\xi = 1,$$

(5.5) 
$$q(-L/2) = q(L/2)$$

after discretization in  $\xi$  for the N+2 variables  $(q, c, \mu)$  using a Newton method. We then add the parameter  $\beta$  as a variable and a standard secant condition to the system (5.2)–(5.5) for numerical continuation in  $\beta$ . We consistently find  $\mu = 0$  to machine precision as expected.

We implement secant continuation starting at  $\beta = 0.3$ , computing profiles and speeds as  $\beta$  varies. In the small- $\beta$  regime, we hold the total mass constant, and, as  $\beta$  approaches 2, we hold the mass of the uniform background state constant, appropriately changing (5.4). The initial interval is of width L = 10 in x, with N = 1030 total grid points. The grid is refined adaptively

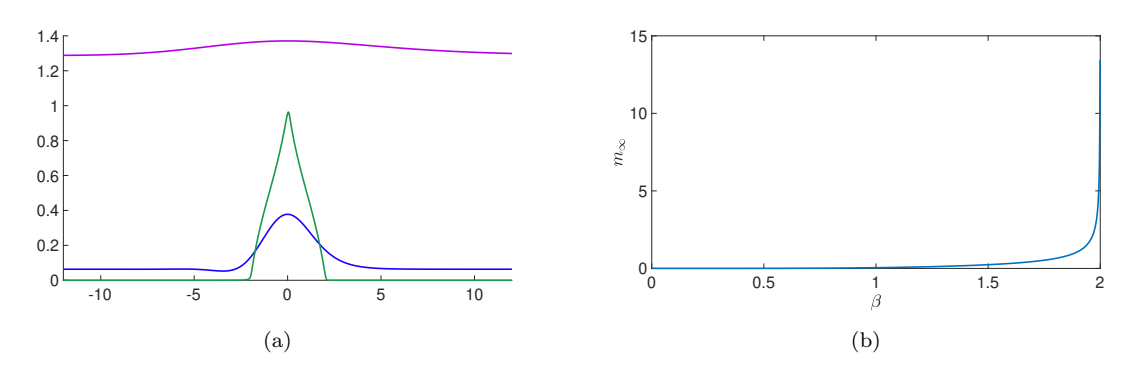
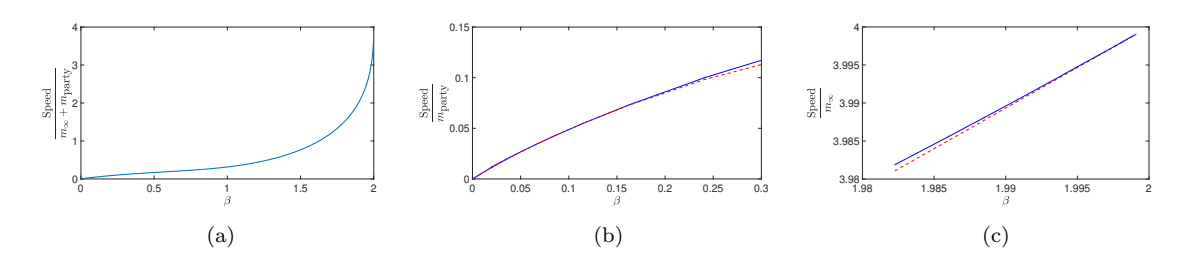


Figure 5.1. (a) Cluster shape for  $\beta = .0006$  (green),  $\beta = 1.08$  (blue), and  $\beta = 1.92$  (purple), with net mass  $m_{\text{cluster}} = 1$ . (b) Plot of  $\beta$  against the value of the uniform background mass  $m_{\infty}$  needed to support a cluster of size 1.



**Figure 5.2.** Numerically computed speed for varying  $\beta$  holding the sum of the background mass and cluster mass constant (a), holding the cluster mass constant (b), and holding the background mass constant (c), with theoretical value shown in red in (b) and (c).

as  $\beta \to 0$  by doubling the number of grid points when the second derivative of q exceeds 0.03 in the sup norm since the profiles develop corners at the peak and sides. As  $\beta \nearrow 2$ , the profiles get increasingly wider. We double the width L of the interval and the number of grid points whenever the number of opinions at distance 0.2L from the center exceeds 0.01 of the peak value. We checked relative discretization and truncation errors by reducing h and increasing L and found errors typically of the order  $10^{-7}$ , always bounded by  $10^{-4}$ .

We see in Figure 5.1(a) three examples of profiles as  $\beta$  varies. We also plot in Figure 5.1(b) the background mass as a function of  $\beta$  when fixing  $\int (q - m_{\infty}) = 1$ , that is, fixing the net mass in the cluster relative to the constant background distribution of opinions. Note that as  $\beta \nearrow 2$  this mass approaches infinity. As  $\beta \to 0$ , the background mass decays exponentially in  $\frac{1}{\beta}$  and therefore is difficult to compute precisely due to limitations in tolerances for the Newton method.

From the secant continuation one also obtains the speed c of the profiles as  $\beta$  varies. In Figure 5.2, we see the relationship between speed and  $\beta$  normalized over total mass, cluster mass, and background mass, respectively. When  $\beta$  is small, we fix the mass of the cluster at 1 and plot the speed, comparing it to its theoretical value from the drift speed calculations, including the numerically computed  $\beta^{3/2}$  correction. As  $\beta$  approaches 2, we fix the uniform background mass and compare the speed with its theoretical value calculated in section 4.3. In all cases, we find excellent quantitative agreement with the leading-order predictions.

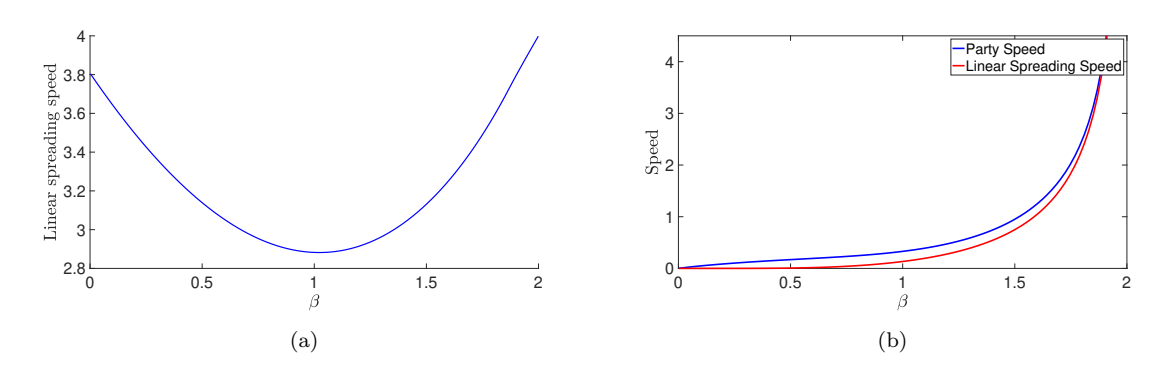


**Figure 5.3.** (a) Spreading speed of instabilities for  $\beta \in [0,2]$  for m=1; (b) cluster speed (blue) and linear spreading speed (red) for  $\beta \in [0,2]$ , with  $m=m_{\infty}(\beta)$ .

5.2. Stability: Direct simulations, convective stability, and pushed fronts. Since the uniform background state of a drifting cluster is unstable for  $0 < \beta < 2$ , drifting clusters will typically not be stable in a strict sense. In fact, the instability of the background state is reflected in unstable continuous spectrum of the linearization. One then would wish to determine whether the instability in the background affects the traveling cluster, that is, whether perturbations grow locally in a vicinity of the cluster or whether they are advected away from the center of the cluster, decaying locally uniformly while growing in norm. This distinction is commonly referred to as the difference between an absolute instability, where perturbations grow locally, and a convective instability, where perturbations decay locally uniformly in the frame comoving with the cluster.

To a good approximation, this question is answered by comparing the spreading speed of perturbations of the uniform state  $P_n = m_{\infty}$ ,  $n \in \mathbb{Z}$ , with the speed of the traveling cluster. Spreading speeds, in most scenarios, are determined as pulled or pushed speeds. In the case of pulled speeds, the spreading is determined by the linear equation, whereas for pushed speeds, the nonlinearity accelerates the propagation. We therefore start with the computation of the linear, pulled spreading speed; see [40, 24, 5] for background and spreading in the nonbiased case. In fact, spreading is mediated by pulled fronts, at the pulled, linear spreading speed, in the nonbiased case as demonstrated in [5].

Recall the dispersion relation for the linearized equation at the uniform state  $P_i \equiv m$ ,

$$-i\omega = m(-2\cos(2\sigma) + (4+2\beta)\cos(\sigma) - (2+2\beta) + i\beta\sin(\sigma)).$$

Then, through a saddle point analysis [40, 5], the linear propagation velocity for any given  $\beta$  is given by

(5.6) 
$$v = \frac{d\omega}{d\sigma} = \frac{\text{Im}[\omega]}{\text{Im}[\sigma]}$$

after solving the second, complex equation for the complex variable  $\sigma \in \mathbb{C}$ . Figure 5.3(a) shows the numerical speeds v, with  $\beta \in [0,2]$  and m=1, and Figure 5.3b compares this linear spreading speed for  $m=m_{\infty}(\beta)$  with the cluster speed.

We find that the linear spreading speed of instabilities is less than the speed of the cluster for  $\beta \in (0,2)$ , which suggest that the cluster is linearly convectively unstable.

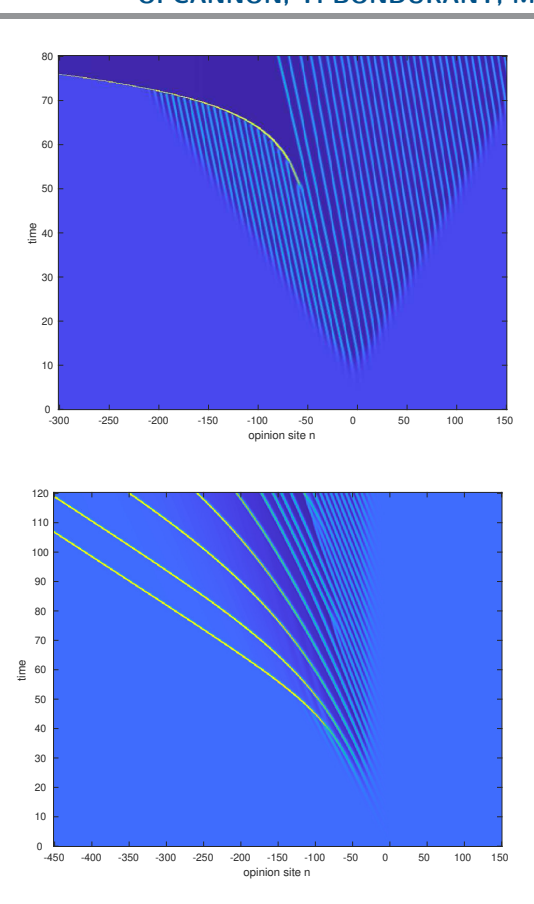


**Figure 5.4.** Space-time plots for  $\beta = .35$  (top) and  $\beta = 0.95$  (bottom), with the initial instability at n = 0. Lighter colors represents higher magnitude.

We explore the possibility of a nonlinear instability, mediated by an analogue of a pushed front, through direct simulations. There, we do see evidence of faster than linear propagation. We simulate (2.2) in an adaptively moving frame in order to compute the spreading speed of instabilities, initializing at a small localized perturbation of the uniform state  $P_i \equiv 1$ . For all  $\beta$ , we see evidence of transient pulled fronts in the wake, which give way to sequences of clusters traveling at a larger than linear speed. The initial transient of pulled front propagation is longer for smaller values of  $\beta$ . The effect is shown in space-time plots (in a stationary frame) with initial conditions given as localized, small perturbations at n=0 of a uniform state m=1. The transient pulled front is most clearly visible in the first plot,  $\beta=0.35$ , where we see a large single traveling cluster begin to form at t=50 and overtake the pulled front at t=75. As  $\beta$  increases, the transient pulled front has a narrow wake and is quickly reached by a large cluster that forms in its wake. In the right panel of Figure 5.4, the pulled front is visible from about t=10 to t=50. In this right panel, one also sees that after the initial nucleation of a large cluster that overtakes the pulled front, more large clusters subsequently form spreading with similar speeds larger than the linear speed. The same effect occurs for smaller values of  $\beta$ , albeit on larger time scales.

In conclusion, we suspect that the traveling clusters are convectively stable, that is, observable, for long transients. The nonlinear process in the wake ultimately results in the creation of a train of traveling clusters of comparable size, which remain well separated, traveling at similar speeds.

A complete description of dynamics, either on a constant background or on a zero background with resulting loss of mass, appears quite intricate. The space-time plots presented here suggest a similarity with phenomena observed in excitable media in simulations and experiments, coined tracefiring and backfiring [7, 32], both of which are also poorly understood mathematically.

- 6. Noncoherence for other bias terms. Different bias mechanisms can generate dynamics very different from the dynamics in (2.2) that we analyzed thus far. We present here briefly phenomena caused by two other forms of bias, namely bias in the compromise process and linear bias mimicking a transport term. The former can be thought of as introducing bias in the compromise process itself rather than through a separate mechanism, and the latter can be thought of as adding bias independent of interaction altogether, neither between sites nor at the same site. For the former, propagation is blocked at one-site clusters; for the latter, we find diffusive dissipation of the cluster, similar to the dynamics of the bounded confidence model with diffusion studied in [4]. We think of those two scenarios as evidence that the self-incitement mechanism of (2.2) is rather special in allowing coherent movement.
- **6.1.** Bias in the compromise process. A natural mechanism for introducing bias would be in the compromise process itself, that is, to consider an equation such as

(6.1) 
$$\frac{dP_n}{dt} = (2 - \beta)P_{n+1}P_{n-1} - (1 - \beta)P_nP_{n+2} - P_nP_{n-2},$$

where agents interact in the same way as in (2.1), but the probability of changing the opinion to the compromise opinion is not equal for the two interacting agents. Another formulation is to include bias in nearest-neighbor interactions and consider the equation

(6.2) 
$$\frac{dP_n}{dt} = 2P_{n+1}P_{n-1} - P_n(P_{n+2} + P_{n-2}) + \beta(P_{n+1}P_n - P_nP_{n-1}),$$

where nearest-neighbor interactions lead to agents moving to the left with probability  $\beta$ . The bias in (6.1) would represent a preference toward compromise in one direction, where agents interacting with more extreme agents within the confidence bound always compromise, but only a fraction  $\beta$  of the time do they compromise when interacting with more moderate agents. In the limiting case  $\beta = 1$ , agents compromise exclusively with more extreme agents. The term in (6.2) would represent asymmetric pull of nearest-neighbor interactions, preferentially toward one end of the opinion spectrum. Reasons for asymmetry might include social comparison or agents thinking it is beneficial to have a more extreme opinion, confirmation bias, self-selection, or preferential interactions. The important distinction is that it is interactions with neighbors at different sites which drive shifts of opinion.

For both (6.1) and (6.2), the bias does not induce persistent drift of existing clusters. In fact, one- and two-site clusters are also equilibria of (6.1), and one-site clusters are equilibria of (6.2). As a result, clusters do not drift at all in (6.1). In (6.2), one can mimic the analysis

in section 3 and find a drift speed near two-site clusters, which vanishes at one-site clusters. The result agrees well with direct numerical simulations which find two-site clusters evolving towards one-site clusters, which are one-sided stable, similar to saddle-node equilibria. One can think of this blocking of motion at one-site clusters as a pinning phenomenon, reflecting the discreteness of the opinion space, similar to the rather well understood pinning of front and pulse propagation in discrete or inhomogeneous media [1].

We note, however, that the dynamics in (6.2) resulting from the perturbation of a spatially constant equilibrium with the resulting formation of multiple clusters is rather complex and does involve movement of clusters, but at nonconstant speeds, mediated by both the bias effect on single clusters and the interaction between clusters.

**6.2. Nonincitement bias.** All bias terms considered thus far are quadratic, modeling person-to-person interactions, and preserve the quadratic scaling invariance of the dynamics. The arguably simplest possible bias terms would model spontaneous change of opinion in one direction, without the need for interaction between agents, and thus be represented by a linear term of the form  $\beta(P_{n+1}-P_n)$ , with variants  $\beta(P_{n+\ell}-P_n)/\ell$ ,  $\ell=2,3,\ldots$  This term would represent a shift in opinion that is not dependent on the population at the opinion site and does not come from any kind of interaction. One could think of this as modeling, for instance an external influence, either informational or parasocial, which affects agents individually and independently of their opinions. Up to scaling, this term can also be viewed as a spatial discretization of the shift term  $u_t = u_x$  in a continuous opinion space  $x \in \mathbb{R}$ . The resulting equation is

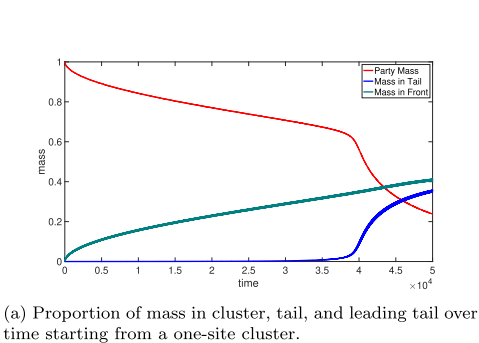
(6.3) 
$$\frac{dP_n}{dt} = 2P_{n+1}P_{n-1} - P_n(P_{n+2} + P_{n-2}) + \beta(P_{n+\ell} - P_n)/\ell,$$

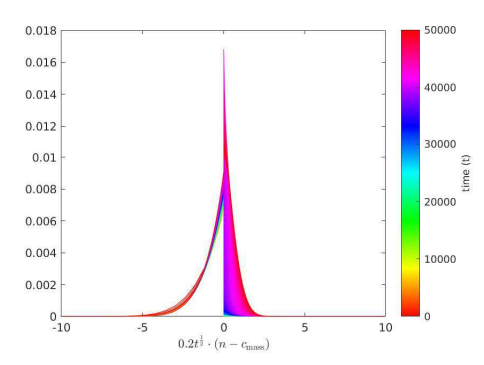
with several possible scalings depending on initial conditions. Numerically, we observe drift of single clusters as expected, with initial speed  $\beta$  at leading order. Expanding the one-sided difference  $P_{n+1} - P_n$  into derivatives, we find at second order an effective diffusion, which indeed is observable in the dynamics and leads to mass loss in the cluster similar to the observations in [4]. Figure 6.1(a) shows the loss of mass from the cluster, defined as all opinions within five sites of the peak, into the tail and leading edge over time. Figure 6.1(b) shows the self-similar shape of the leading edge when scaled horizontally by  $t^{-\frac{1}{2}}$ , mimicking the profiles in [4]. The tail, however, appears to grow exponentially in time at first and then becomes diffusive as the mass of the cluster is no longer significant; see also Figure 6.1(a). The effect of mass loss can also be understood in the small- $\beta$  perturbation analysis of section 3, where at higher order, the drift term generates growth at sites with distance 3 or more to the cluster. In fact, for long-range coupling  $\ell > 2$ , the effect appears at first order in  $\beta$  and the mass loss is correspondingly more pronounced.

6.3. Stability of uniform opinion distribution in the presence of different forms of bias. The effect of bias for our original model of quadratic self-incitement  $-\beta P_n^2$  leads to stabilization of uniform opinion distributions for strong enough bias  $\beta > 2$ . The effect in the forms of bias discussed in this section also differs in this aspect.

For the biased compromise process (6.1), the linear dispersion relation at a constant state  $P_n \equiv m$  is

$$(6.4) \lambda = m \left( 4\cos(\sigma) - 2\cos(2\sigma) - 2 + \beta(1 - 2\cos(\sigma) + \cos(2\sigma) + i\sin(2\sigma)) \right),$$





(b) Profiles of the leading and trailing tails, omitting the main cluster in between, with the opinion space scaled by  $t^{\frac{1}{2}}$ 

**Figure 6.1.** Plot of proportion of mass in the cluster, tail, and leading tail over time and profiles of the tails plotted against  $t^{\frac{1}{2}} \cdot n$ .

with  $0 \le \beta \le 1$  representing the physically feasible parameter region since  $\beta$  is the fraction of interactions leading to compromise toward the unfavored direction. One finds that the stability of the constant state is unchanged from (2.1); the uniform state remains unstable for all  $0 \le \beta \le 1$ . In other words, for this model, the bias cannot compensate for the instability from the compromise process.

For biased nearest-neighbor compromise (6.2), the linear dispersion relation at a constant state is

(6.5) 
$$\lambda = m \left( 4\cos(\sigma) - 2\cos(2\sigma) - 2 + \beta(2i\sin(\sigma)) \right)$$

for  $0 \le \beta$ . Here, the effect of bias is purely advective-dispersive, and again, the uniform state is always unstable for  $\beta \ge 0$ . Again, no strength of bias can stabilize the constant state.

Finally, for (6.3), the linear dispersion relation at the uniform state is

(6.6) 
$$\lambda = m \left( 4\cos(\sigma) - 2\cos(2\sigma) - 2 + \frac{\beta}{m}(\cos(\sigma) - 1 + i\sin(\sigma)) \right).$$

In this case, we do see stabilization of the uniform state above a threshold that depends on its magnitude,  $\beta_{\text{crit}} = 4m$ . In this way, the effect is similar to the effect of self-incitement, but also notably different—for self-incitement, bias above the critical level  $\beta_{\text{crit}} = 2$  stabilizes a uniform state of any magnitude, but for (6.3), larger and larger bias is required as the population increases. We do note that stabilization of the uniform distribution is well known in the context of noisy opinion dynamics and models with discrete diffusion [4, 10], and there also, higher noise is required as the population increases. The above findings for (6.3) are thus not unexpected if interpreting the bias as a one-sided diffusive process.

**7. Discussion.** We presented results on the effect of bias in a deterministic bounded confidence model. The corresponding unbiased bounded confidence model supports localized clusters, including a one-parameter family roughly parameterized by the position of the cluster in space. One expects that introduction of bias leads to a drifting movement of clusters. We analyze this drifting motion in two limits, small and large bias. For large bias,

 $\beta > 2$ , we find that the uniform distribution is stable, preventing cluster formation and polarization. For bias close to but below threshold,  $\beta \lesssim 2$ , we prove that coherent movement of clusters on a constant background distribution of opinions is possible for quadratic self-incitement bias. Numerically, we find such coherent motion for all values of bias  $0 < \beta < 2$ . For small values of  $\beta$ , the constant background distribution is exponentially small in the parameter and drift speeds are obtained from a leading-order analysis of the flow on a slow manifold.

Technically, we used a geometric singular perturbation analysis to derive drift speeds in the small bias regime and a nonlocal center manifold analysis to find coherent drifting clusters for  $\beta \lesssim 2$ . The analysis in the latter case is possibly of independent interest, demonstrating the simplicity of calculations in the recently introduced framework of center manifolds without a phase space. Within the narrow focus on coherent drifting clusters, a major open question is to establish rigorously existence, drift speeds, and size of background state in the regime  $\beta \gtrsim 0$ .

Beyond coherent drifting clusters, we touched on the evolution near unstable constant states. We find modulation equations familiar from fluid dynamics, such as the Korteweg–de Vries or the Kuramoto–Sivashinsky equation and variations thereof. Observed dynamics in simulations appear to involve complex dynamics of formation and interaction of clusters.

Interesting questions arise when attempting to quantify mass loss in incoherent drifting clusters. Geometric singular perturbation theory at a single cluster predicts mass accumulation in sites further away from the center of the cluster, possibly at high or beyond all orders in  $\beta$  depending on the bias term. It would be interesting to quantify these effects and, for quadratic self-incitement bias, to contrast with the existence of coherent drifting clusters on a constant background, relating, for instance, the size of the constant background to the rate of mass loss.

We noted that stability questions in the context of bias are subtle due to the instability of the constant background state and the complexity of the dynamics in the evolution of perturbations. In fact, it appears that even without bias, stability of clusters against perturbations, say small in  $\ell^{\infty}$ , is not known. On the other hand, we expect that one should be able to establish nonlinear stability of the constant state for large bias base against, say, small perturbations in  $\ell^{1}$  using the heat-equation-type linear decay and a fixed point argument that exploits discrete derivatives in the nonlinearity.

We note that some of the effects of bias studied here are strongly tied to the fact that discrete transport is inherently diffusive and dispersive, as seen, for instance, in the Fourier symbol  $e^{i\sigma} - 1 \sim i\sigma - \sigma^2 - i\sigma^3$  of the discrete derivative  $P_{j+1} - P_j$ . In a model with continuous opinion distributions, diffusive and dispersive effects could be avoided by adding a simple drift term  $\partial_x P$ . More in the spirit of the bounded confidence model would, however, be a nonlocal bias K \* P with asymmetric convolution kernel K, which in turn would introduce similar diffusive-dispersive effects through nonvanishing second and third moments of the interaction kernel K. In that regard, the discrete opinion space simply enforces a nonlocality in the interaction, not different from the continuous model. It would be interesting to explore the effect of such a nonlocal bias on drift of opinion clusters in this context, exploring in particular localization of clusters in comparison to the Dirac- $\delta$  localization in the absence of bias.

## REFERENCES

- N. Ankney, M. Avery, T. Khain, and A. Scheel, Pinning and depinning: From periodic to chaotic and random media, Chaos, 29 (2019), 013127.
- B. Bakker and A. Scheel, Spatial Hamiltonian identities for nonlocally coupled systems, Forum Math. Sigma, 6 (2018), e22.
- [3] P. W. Bates, K. Lu, and C. Zeng, Approximately invariant manifolds and global dynamics of spike states, Invent. Math., 174 (2008), pp. 355-433.
- [4] E. Ben-Naim, Opinion dynamics: Rise and fall of political parties, Europhys. Lett. EPL, 69 (2005), pp. 671–677.
- [5] E. Ben-Naim and A. Scheel, Pattern selection and super-patterns in opinion dynamics, in APS March Meeting Abstracts, Vol. 2016, 2016, X43.006.
- [6] V. D. BLONDEL, J. M. HENDRICKX, AND J. N. TSITSIKLIS, On Krause's multi-agent consensus model with state-dependent connectivity, IEEE Trans. Automat. Control, 54 (2009), pp. 2586–2597.
- [7] G. Bordyugov and H. Engel, Anomalous pulse interaction in dissipative media, Chaos, 18 (2008), 026104.
- [8] J. Bricmont, A. Kupiainen, and G. Lin, Renormalization group and asymptotics of solutions of non-linear parabolic equations, Comm. Pure Appl. Math., 47 (1994), pp. 893–922.
- [9] T. CARLETTI, D. FANELLI, S. GROLLI, AND A. GUARINO, How to make an efficient propaganda, Europhys. Lett. EPL, 74 (2007), 222.
- [10] B. CHAZELLE, Q. JIU, Q. LI, AND C. WANG, Well-posedness of the limiting equation of a noisy consensus model in opinion dynamics, J. Differential Equations, 263 (2017), pp. 365–397.
- [11] S. CHEN, D. H. GLASS, AND M. MCCARTNEY, Characteristics of successful opinion leaders in a bounded confidence model, Phys. A, 449 (2016), pp. 426–436.
- [12] M. DEL VICARIO, A. SCALA, G. CALDARELLI, H. STANLEY, AND W. QUATTROCIOCCHI, Modeling confirmation bias and polarization, Sci. Rep., 7 (2017), 40391.
- [13] A. Doelman, B. Sandstede, A. Scheel, and G. Schneider, *The dynamics of modulated wave trains*, Mem. Amer. Math. Soc., 199 (2009), 934.
- [14] I. DOUVEN AND R. HEGSELMANN, Mis- and disinformation in a bounded confidence model, Artificial Intelligence, 291 (2020), 103415.
- [15] G. FAYE AND A. SCHEEL, Fredholm properties of nonlocal differential operators via spectral flow, Indiana Univ. Math. J., 63 (2014), pp. 1311–1348.
- [16] G. FAYE AND A. SCHEEL, Center manifolds without a phase space, Trans. Amer. Math. Soc., 370 (2018), pp. 5843–5885.
- [17] N. FENICHEL, Persistence and smoothness of invariant manifolds for flows, Indiana Univ. Math. J., 21 (1971/72), pp. 193–226.
- [18] S. FORTUNATO, V. LATORA, A. PLUCHINO, AND A. RAPISARDA, Vector opinion dynamics in a bounded confidence consensus model, Internat. J. Modern Phys. C, 16 (2005), pp. 1535–1551.
- [19] W. Han, C. Huang, and J. Yang, Opinion clusters in a modified Hegselmann-Krause model with heterogeneous bounded confidences and stubbornness, Phys. A, 531 (2019), 121791.
- [20] R. HEGSELMANN AND U. KRAUSE, Opinion dynamics and bounded confidence models, analysis and simulation, J. Artif. Soc. Soc. Simul., 5 (2002).
- [21] D. HENRY, Geometric Theory of Semilinear Parabolic Equations, Lecture Notes in Math. 840, Springer-Verlag, Berlin, New York, 1981.
- [22] M. W. HIRSCH, C. C. PUGH, AND M. SHUB, Invariant Manifolds, Lecture Notes in Math. 583, Springer-Verlag, Berlin, New York, 1977.
- [23] M. HOLZER AND R. KHATRI, Pattern formation, traveling fronts and consensus versus fragmentation in a model of opinion dynamics, Phys. Lett. A, 381 (2017), pp. 3197–3202.
- [24] M. HOLZER AND A. SCHEEL, Criteria for pointwise growth and their role in invasion processes, J. Non-linear Sci., 24 (2014), pp. 661–709.
- [25] D. J. ISENBERG, Group polarization: A critical review and meta-analysis, J. Pers. Soc. Psychol., 50 (1986), pp. 1141–1151.
- [26] G. IYER AND H. YOGANARASIMHAN, Strategic polarization in group interactions, J. Mark. Res., 58 (2021), pp. 782–800.

- [27] J. Kertesz, A. Sirbu, F. Gianotti, and D. Pedreschi, Algorithmic bias amplifies opinion polarization: A bounded confidence model, in StatPhys 27 Main Conference, 2019.
- [28] M. KRUPA AND P. SZMOLYAN, Extending slow manifolds near transcritical and pitchfork singularities, Nonlinearity, 14 (2001), pp. 1473–1491.
- [29] J. LORENZ, Continuous opinion dynamics under bounded confidence: A survey, Internat. J. Modern Phys. C, 18 (2007), pp. 1819–1838.
- [30] J. LORENZ, A stabilization theorem for dynamics of continuous opinions, Phys. A, 355 (2005), pp. 217–223.
- [31] E. C. MAIN AND T. G. WALKER, Choice shifts and extreme behavior: Judicial review in the federal courts, J. Soc. Psychol., 91 (1973), pp. 215–221.
- [32] N. Manz and O. Steinbock, Propagation failures, breathing pulses, and backfiring in an excitable reaction-diffusion system, Chaos, 16 (2006), 037112.
- [33] J.-D. Mathias, S. Huet, and G. Deffuant, Bounded confidence model with fixed uncertainties and extremists: The opinions can keep fluctuating indefinitely, J. Artif. Soc. Soc. Simul., 19 (2016), 6.
- [34] D. G. MYERS, Polarizing effects of social comparison, J. Exp. Soc. Psychol., 14 (1978), pp. 554-563.
- [35] D. G. Myers and H. Lamm, The group polarization phenomenon, Psychol. Bull., 83 (1976), pp. 602-627.
- [36] W. Quattrociocchi, G. Caldarelli, and A. Scala, Opinion dynamics on interacting networks: Media competition and social influence, Sci. Rep., 4 (2014), 4938.
- [37] G. Schneider and C. E. Wayne, Counter-propagating waves on fluid surfaces and the continuum limit of the Fermi-Pasta-Ulam model, in International Conference on Differential Equations, Vols. 1, 2 (Berlin, 1999), World Scientific, River Edge, NJ, 2000, pp. 390–404.
- [38] D. Shen and Z. Sun, Finite-time convergence of KH model under asymmetric confidence levels, in Proceedings of the IEEE International Conference on Control and Automation, 2009, pp. 224–227.
- [39] C. R. Sunstein, The law of group polarization, J. Political Philos., 10 (2002), pp. 175–195.
- [40] W. VAN SAARLOOS, Front propagation into unstable states, Phys. Rep., 386 (2003), pp. 29–222.
- [41] L. Van Swol, Extreme members and group polarization, Soc. Influ., 4 (2009), pp. 185-199.
- [42] A. VANDERBAUWHEDE AND G. IOOSS, Center manifold theory in infinite dimensions, in Dynamics Reported: Expositions in Dynamical Systems, Dynam. Report. Expositions Dynam. Systems (N.S.) 1, Springer, Berlin, 1992, pp. 125–163.
- [43] M. Zhang, X. Ma, W. Chen, and H. Lan, Group polarization in board decisions about strategic change: Evidence from Chinese publicly listed companies (2008-2018), Manag. Organ. Rev., 19 (2023), pp. 201–232.